

AN INVESTIGATION OF THE NEUTRINO OSCILLATION IN THE  
NEUTRINO-DOMINATED ACCRETION FLOWS  
AROUND A BLACK HOLE



A Thesis Submitted in Partial Fulfillment of the Requirements for the  
Degree of Master of Science in Physics  
Suranaree University of Technology  
Academic Year 2023

การศึกษาการสั้นของนิวตริโนในระบบงานพอกพูนมวล  
ที่ปกคลุมด้วยนิวตริโนรอบหลุมดำ



วิทยานิพนธ์นี้เป็นส่วนหนึ่งของการศึกษาตามหลักสูตรปริญญาวิทยาศาสตรมหาบัณฑิต  
สาขาวิชาฟิสิกส์  
มหาวิทยาลัยเทคโนโลยีสุรนารี  
ปีการศึกษา 2566


AN INVESTIGATION OF THE NEUTRINO OSCILLATION IN THE NEUTRINO-  
DOMINATED ACCRETION FLOWS AROUND A BLACK HOLE

Suranaree University of Technology has approved this thesis submitted in  
partial fulfillment of the requirements for a Master's Degree.

Thesis Examining Committee

  
\_\_\_\_\_  
(Assoc. Prof. Dr. Patipan Uttayarat)

Chairperson

  
\_\_\_\_\_  
(Assoc. Prof. Dr. Poemwai Chainakun)

Member (Thesis Adviser)

  
\_\_\_\_\_  
(Prof. Dr. Yupeng Yan)


Member


  
\_\_\_\_\_  
(Dr. Warintorn Sreethawong)

Member

  
\_\_\_\_\_  
(Asst. Prof. Dr. Tirawut Worrakitpoonpon)

Member

  
\_\_\_\_\_  
(Assoc. Prof. Dr. Yupaporn Ruksakulpiwat)  
Vice Rector for Academic Affairs  
and Quality Assurance

  
\_\_\_\_\_  
(Prof. Dr. Santi Maensiri)  
Dean of Institute of Science

ชิตพัทธ์ ดีเสมอ : การศึกษาการสั่นของนิวตริโนในระบบจานพอกพูนมวลที่ปกคลุมด้วยนิวตริโนรอบหลุมดำ (AN INVESTIGATION OF THE NEUTRINO OSCILLATION IN THE NEUTRINO-DOMINATED ACCRETION FLOWS AROUND A BLACK HOLE) อาจารย์ที่ปรึกษา : รองศาสตราจารย์ ดร.เพิ่มวัย ชัยนะกุล, 43 หน้า.

คำสำคัญ : จานพอกพูนมวล, ฟิสิกส์หลุมดำ, นิวตริโน

เราศึกษาผลของการสั่นของนิวตริโนต่อความส่องสว่างของนิวตริโน (แอนไทนิวตริโน) และความส่องสว่างของการประลัย ในระบบจานพอกพูนมวลที่ปกคลุมด้วยนิวตริโน หรือ โมเดลระบบระบายความร้อนของนิวตริโนบนจานพอกพูนมวลรอบหลุมดำมวลเทียบเท่าดวงอาทิตย์ เราใช้ผลเฉลยจากการศึกษาก่อน ๆ เพื่อจำลองโมเดลแบบง่ายและลดเวลาในการคำนวณ โดยตั้งเงื่อนไขขอบเขตที่มีผลของสถานะเสื่อมของอิเล็กตรอนและผลของการกักขังนิวตริโนเพื่อการคำนวณในขอบเขตรัศมีที่กำหนด  $r = 1.473-500 r_g$  ซึ่งเราได้ทำการทดสอบโมเดลด้วยสองพารามิเตอร์หลัก: อัตราการพอกพูนมวล ( $\dot{M} = 0.1-10 \dot{M}_E s^{-1}$ ) และค่าการหมุนของหลุมดำ ( $a = 0-1$ ) จากผลการทดลอง พบว่าในสถานการณ์ที่ไม่มีผลของการสั่นของนิวตริโน ความส่องสว่างของนิวตริโนอยู่ที่  $10^{51}-10^{53} \text{ erg s}^{-1}$  และความส่องสว่างของการประลัยอยู่ที่  $10^{50}-10^{55} \text{ erg s}^{-1}$  โดยความส่องสว่างประลัยนี้จะเพิ่มขึ้นประมาณ 12-20% เมื่อคิดผลของการสั่นของนิวตริโน แต่อย่างไรก็ตามจะเห็นได้ชัดว่ามีวอนนิวตริโนมีการลดลงน้อยกว่าหรือเท่ากับ 8% โดยประมาณจากการสั่นของนิวตริโน ในขณะที่อิเล็กตรอนนิวตริโน และเทานิวตริโนมีการเพิ่มขึ้นได้มากถึง 34% และสุดท้ายนี้ เราได้ศึกษาผลของการละเมิดของประจุและสมมาตรในการสั่นของนิวตริโน โดยมีผลต่างของเฟส  $\delta CP$  เท่ากับ  $0^\circ$  และ  $245^\circ$  รวมถึงพิจารณาถึงผลกระทบนี้ต่อการสั่นของนิวตริโน

สาขาวิชาฟิสิกส์  
ปีการศึกษา 2566

ลายมือชื่อนักศึกษา ชิตพัทธ์ ดีเสมอ  
ลายมือชื่ออาจารย์ที่ปรึกษา Poemuni Chainah

CHITIPAT DEESAMER : AN INVESTIGATION OF THE NEUTRINO OSCILLATION IN  
THE NEUTRINO-DOMINATED ACCRETION FLOWS AROUND A BLACK HOLE. THESIS  
ADVISOR : ASSOC. PROF. POEMWAI CHAINAKUN, Ph.D. 43 PP.

Keyword: Accretion, Black hole, Neutrino

We investigate the effect of neutrino oscillation on the neutrino (anti-neutrino) luminosity and the annihilation luminosity of neutrino-dominated accretion flow (NDAF), or the model of neutrino cooling accretion disk around stellar-mass black hole. To simplify the model and decrease time consumption, we then adopt the empirical hydrodynamics solution of the disk from previous studies. The boundary conditions, including the effect of electron degeneracy and neutrino trapping, are used for a limited calculation in the fixed radial distance  $r = 1.473\text{--}500 r_g$ . The model is tested with two key parameters: mass accretion rate ( $\dot{M} = 0.1\text{--}10 \dot{M} s^{-1}$ ) and black hole spin ( $a = 0\text{--}1$ ). In the absence of neutrino oscillation, we obtain neutrino/anti-neutrino luminosity of about  $10^{51}\text{--}10^{53} \text{ erg s}^{-1}$ , and consequently, neutrino annihilation luminosity of about  $10^{50}\text{--}10^{55} \text{ erg s}^{-1}$ . With the neutrino oscillation in the vacuum limit, we found that the total annihilation luminosity can rise by  $\sim 12\text{--}20\%$ . However, it is noticeable that muon neutrino annihilation luminosity decreases by  $\lesssim 8\%$  in the flavor transition process, while the electron- and tau-neutrino luminosities potentially increase up to  $\sim 34\%$ . Finally, we also investigate the distinction between the CP-violating phase of the oscillation, where  $\delta_{CP} = 0^\circ$  and  $245^\circ$ , and discuss the impact on neutrino annihilation luminosity.

School of Physics  
Academic Year 2023

Student's Signature चितิปัทธ์ ดีธรรม  
Advisor's Signature Poemwai Chainakun

## ACKNOWLEDGEMENT

Sincerely speaking, I would like to express deep respect to my supervisor, Assoc. Prof. Dr. Poemwai Chainakun, for always providing me with ideas and opinions, and guiding me to the decisive decision in order to succeed in my work. This work would not have been possible without his lots of efforts.

Many thanks to my friends, who cherished our time and supported me in many ways and my School of Physics colleagues who are always willing to give some useful advice.

Lastly, I wish to express gratitude for the financial assistance received through the scholarship provided by the Thai government under the Development and Promotion of Science and Technology Talents Project, administered by the Institute for the Promotion of Teaching Science and Technology (IPST). This funding has been instrumental in facilitating the execution of my research project, enabling me to secure essential resources and advance my academic pursuits.

มหาวิทยาลัยเทคโนโลยีสุรนารี

Chitipat Deesamer

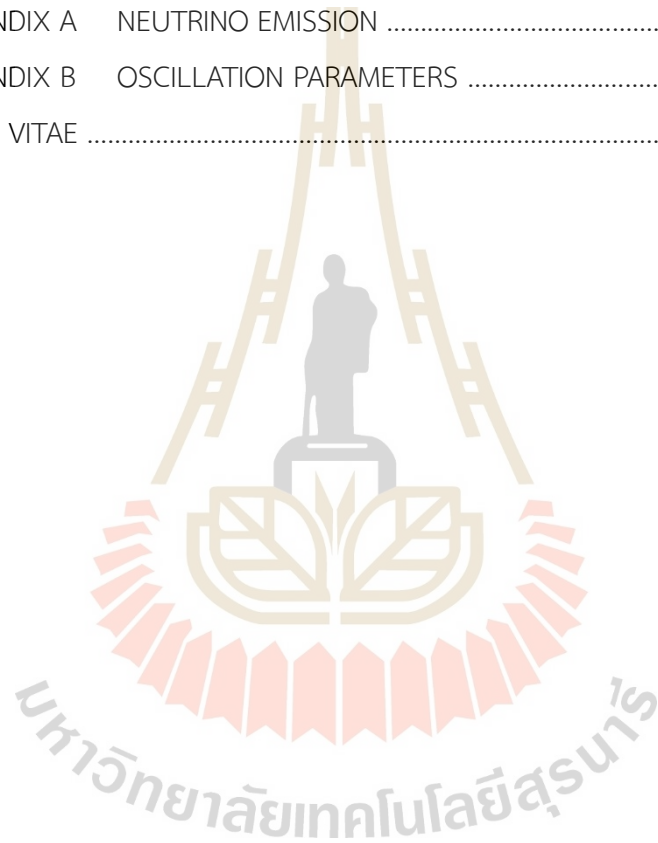
# CONTENTS

	Page
ABSTRACT IN THAI .....	I
ABSTRACT IN ENGLISH .....	II
ACKNOWLEDGEMENTS .....	III
CONTENTS .....	IV
LIST OF TABLES .....	VI
LIST OF FIGURES .....	VII
LIST OF ABBREVIATIONS .....	VIII
<b>CHAPTER</b>	
<b>I INTRODUCTION .....</b>	<b>1</b>
<b>II LITERATURE REVIEW .....</b>	<b>3</b>
2.1 Fundamental and discovery of neutrino .....	3
2.1.1 Neutrino in the Standard Model .....	3
2.1.2 Discovery of neutrino .....	4
2.2 NDAF black hole .....	7
2.2.1 History of NDAF model .....	7
2.2.2 Neutrino oscillation on NDAF .....	10
<b>III METHODOLOGY .....</b>	<b>11</b>
3.1 Geometry and Model Assumptions .....	11
3.2 Disk Temperature and Density Profile .....	13
3.3 Cooling Processes and Luminosity .....	14
3.4 Annihilation Luminosity .....	15
3.5 Neutrino Oscillation .....	16



## CONTENTS (Continued)

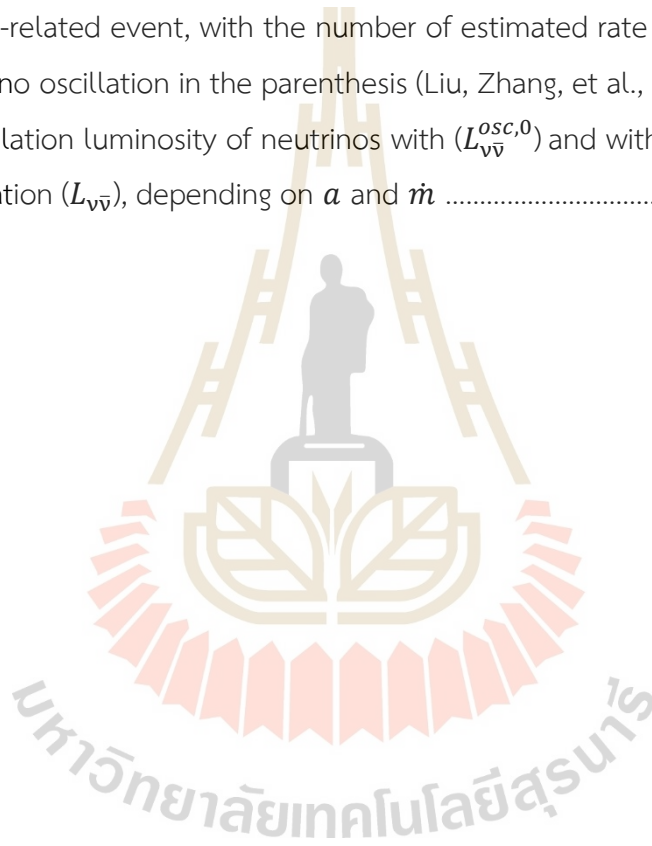
	Page
IV    RESULTS .....	19
V     DISCUSSION AND CONCLUSION .....	26
REFERENCES .....	30
APPENDICES	
APPENDIX A    NEUTRINO EMISSION .....	39
APPENDIX B    OSCILLATION PARAMETERS .....	42
CURRICULUM VITAE .....	43





## LIST OF TABLES

Table		Page
2.1	List of neutrino detectors .....	6
2.2	The detection rate and the optimistic detection rate of electron neutrino, for SN-related event, with the number of estimated rate including neutrino oscillation in the parenthesis (Liu, Zhang, et al., 2016) .....	10
4.1	Annihilation luminosity of neutrinos with ( $L_{\nu\bar{\nu}}^{osc,0}$ ) and without neutrino oscillation ( $L_{\nu\bar{\nu}}$ ), depending on $a$ and $m$ .....	22



## LIST OF FIGURES

Figure	Page
2.1	The handedness of the neutrino ..... 4
2.2	The solar neutrino flux spectrum and energy (MeV). The color code is the efficient energy range of each experiment (Gallium, Chlorine, Super-K & SNO) (Bellerive, 2004) ..... 5
2.3	Schematic picture of characteristic radii of NDAFs (Liu et al., 2017) ..... 9
3.1	Schematic of a simplified neutrino-cooled accretion disk model (not to scale). The disk regions are separated into the trapping region ( $r < r_{\text{trp}}$ ), emission region ( $r_{\text{trp}} < r < r_{\text{ign}}$ ), and outer region ( $r < r_{\text{ign}}$ ) ..... 12
4.1	Disk temperature profiles as a function of $r$ as a continuous function of $r$ ... 19
4.2	Radial profiles of neutrino cooling rate $Q_{\nu} = \sum_i Q_{\nu_i}$ (solid line) and anti-neutrino cooling rate $Q_{\bar{\nu}} = \sum_i Q_{\bar{\nu}_i}$ (dashed line) ..... 20
4.3	Radial profiles of the neutrino luminosity (solid lines) and anti-neutrino luminosity (dashed lines) as a continuous function of $r$ ..... 21
4.4	Relative annihilation luminosity difference $\Delta L_{\nu\bar{\nu}}^{\text{osc}}/L_{\nu\bar{\nu}}$ varying with $\alpha$ and $\dot{m}$ , when $\Delta L_{\nu\bar{\nu}}^{\text{osc}}/L_{\nu\bar{\nu}} = (L_{\nu\bar{\nu}}^{\text{osc},0} - L_{\nu\bar{\nu}})/L_{\nu\bar{\nu}}$ . The CP-violating phase is $\delta CP = 0^\circ$ ..... 23
4.5	Relative annihilation luminosity difference $\Delta L_{\nu\bar{\nu}}^{\text{CP}}/L_{\nu\bar{\nu}}^{\text{osc},0}$ varying with $\alpha$ and $\dot{m}$ , when $\Delta L_{\nu\bar{\nu}}^{\text{CP}}/L_{\nu\bar{\nu}}^{\text{osc},0} = (L_{\nu\bar{\nu}}^{\text{osc},245} - L_{\nu\bar{\nu}}^{\text{osc},0})/L_{\nu\bar{\nu}}^{\text{osc},0}$ and $\delta CP$ changes from $0^\circ$ to $245^\circ$ ..... 24
4.6	Comparison of results in the annihilation luminosity with neutrino oscillation $L_{\nu\bar{\nu}}^{\text{osc},0}$ for $\delta CP = 0^\circ$ (red solid line), and without neutrino oscillation $L_{\nu\bar{\nu}}$ (black solid line) ..... 25

## LIST OF ABBREVIATIONS

$a$	black hole spin where $a = J/mc^2$
BH	black hole
GRB	gamma-ray burst
$\dot{M}$	mass accretion rate
$M_{\odot}$	solar mass
NDAF	neutrino-dominated accretion flow
DUNE	Deep Underground Neutrino Experiment
Hyper-K	Hyper-Kamiokande
JUNO	Jiangmen Underground Neutrino Observatory



มหาวิทยาลัยเทคโนโลยีสุรนารี

# CHAPTER I

## INTRODUCTION

Neutrino is a subatomic particle with a low mass and a neutral charge. These neutrinos can be produced in weak interactions through the decay processes of a particle group named “lepton.” The type of neutrinos is differentiated by those origin leptons, including electron ( $e$ ), muon ( $\mu$ ), and tau ( $\tau$ ). However, its size is relatively small, which makes the interaction effective only at an extremely close distance. Therefore, neutrino physics has become a challenging topic for research in frontier science, especially regarding detection. To understand the existence of neutrinos and their connection in the universe, we still need more precise experimental data, which requires high-performance detectors, i.e., DUNE, Hyper-K, IceCube, JUNO (Falcone and Collaboration, 2022), etc. In addition, this also leads scientists to search for prominent candidate events that could produce an abundance of neutrinos, such as the Big Bang, cosmic rays, and supernovae. Recently, gamma-ray burst (GRB) was proposed as another candidate for MeV-neutrino detection since they are the most explosive events in the universe and can emit a great deal of energy, which may create a vast number of neutrinos (Narayan, Paczynski, and Piran, 1992). However, the origin of the GRB formation remains questionable.

Neutrino-dominated accretion flow (NDAF) around rotating black holes, formed after the collapsar scenario, had been postulated to be the model of the central engine for GRBs (Popham, Woosley, and Fryer, 1999). The significance of this model is the cooling mechanisms of the accretion disk that could release a large number of neutrinos and anti-neutrinos. These particles are emitted from the surface of the accretion disk, then annihilate and form a relativistic outflow above the disk, in which the transferred energy is sufficient to drive the GRB.

After that, there were many studies on this model, and more levels of neutrino physics were taken into account (Kohri, Narayan, and Piran, 2005; W.-X. Chen and Beloborodov, 2007; Xue, Liu, Gu, and Lu, 2013; Liu, Gu, and Zhang, 2017). For observation, the predictions of the detection rate of neutrinos from the GRB driven by the NDAFs were made, and the consequence of the neutrino oscillation effect, which had been neglected before, was mentioned (Liu, Zhang, Li, Ma, and Xue, 2016). This is the phenomenon when neutrinos transform their type into another, there was a consideration of the effect of neutrino oscillation inside the accretion disk, and the results showed a reduction in the neutrino flux in the luminosity calculation (Uribe, Becerra-Vergara, and Rueda, 2021). However, neutrino oscillation may occur above the disk as well as inside the disk. Therefore, both calculations should be considered simultaneously.

In this work, we investigate the effects of neutrino oscillations on the neutrino luminosity and annihilation luminosity at the region above the accretion disk of the NDAF with the neutrino/anti-neutrino pair-annihilation model. To simplify the calculation, we model the hydrodynamic properties adopted from the empirical solution from the previous literature (Kohri et al., 2005; W.-X. Chen and Beloborodov, 2007; Xue et al., 2013; Liu et al., 2017). We define some simple boundary conditions, such as neutrino trapping radius and electron degeneracy, which can determine thermodynamic properties within the specific region of the disk around radial distance  $r = 1.473 - 500 r_g$ . Note that  $r_g = 2GM/c^2$ ,  $G$  is the gravitational constant,  $M$  is the mass of the black holes, and  $c$  is the speed of light. To compare our results to plausible NDAF sources, we investigate our model with two key parameters: mass accretion rate ( $\dot{M}$ ) and black hole spin ( $a$ ). Besides, we test our result with the different phases of neutrino oscillation called the “CP-violating phase.” This phase can differentiate the oscillation between neutrino and anti-neutrino. Finally, we will discuss the impact of neutrino oscillation above the disk on the annihilation luminosity. We expect that our results will provide a more realistic picture of the NDAF black hole model and advance the study to GRB formation.

## CHAPTER II

### LITERATURE REVIEW

In this section, we will discuss the fundamentals of neutrino physics, followed by the discovery of neutrino detection and, remarkable phenomena, neutrino oscillation. Then, we will explain the NDAFs model and the development of this model in the different levels of neutrino physics. Finally, we will discuss the effect of the neutrino oscillation on our model.

#### 2.1 Fundamental and discovery of neutrino

Even though billions of neutrinos pass through our bodies, only a small number of neutrinos could be detected because the range of the interaction is extremely small due to its low mass and no charge. However, this still gives the motivation to the scientist to detect this particle and a lot of detection methods were proposed. The model and history of neutrinos will be explained in the following sub-sections.

##### 2.1.1 Neutrino in the Standard Model

At first, in the Standard Model, neutrino is described for an elementary particle in the lepton group, spin number  $\frac{1}{2}$  (one of the quantum states), with no mass and no charge. The interaction of a neutrino with other particles can be only via weak interaction with two mediators: Z and W boson. In particle physics, there is a relation between the spin and the direction of motion, which is called “Helicity”, described by the handedness (Figure 2.1). In this case, the sign of helicity is defined by whether it’s spin direction is the same (positive, right-handed) or opposite (negative, left-handed) direction as its momentum.

In practice, the handedness of neutrino is used in chirality terms, or the intrinsic properties for transforming particles in chiral symmetry. If the neutrino is massless, the helicity and chirality will be the same (both handedness). However, the conflict occurs when the experiment shows that only left-handed neutrinos are measurable. Therefore, this indicates that neutrinos should be massive instead, and later, in neutrino physics, will be described in term of Dirac mass  $\mathcal{L}_{Dirac} = -\bar{\nu}\widehat{M}\nu' = -\sum_{i=1}^3 m_i \bar{\nu}_i \nu_i$ , or Majorana mass,  $\mathcal{L}_{Majorana} = \frac{1}{2} m_M \bar{\psi}\psi$ .

With this assumption, ones would seek the nature of neutrinos and study their behavior. The discovery in neutrino physics will be explained in the next sections.

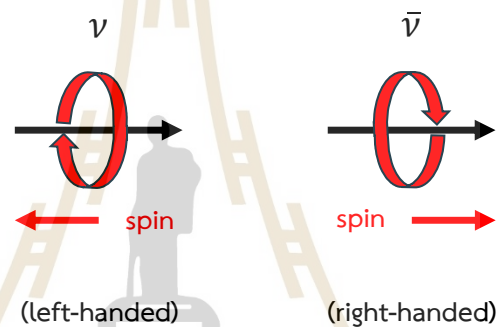


Figure 2.1 The handedness of the neutrino.

### 2.1.2 Discovery of neutrino

In our universe, neutrinos can be produced from various decays via weak interaction, but the most important reaction is beta decay, introduced by Wolfgang Pauli in 1930. This process is obtained by balancing the chemical process of the nucleus that releases electron, with the invincible positive lepton number. To fulfill the laws of conservation of physics properties, the addition of a tiny particle in opposite sign of lepton number was included, and later the positive one was called neutrino (and anti-neutrino, which has negative lepton number).

Neutrino has gained more interest since the observation of electron anti-neutrino, from nuclear reactor, was discovered in the Reines-Cowan experiment in 1956 (Cowan, Reines, Harrison, Kruse, and McGuire, 1956). This also provided the first evidence of the existence of neutrinos. At the same time, the theory of neutrino oscillation was proposed by Bruno Pontecorvo, and was mentioned that neutrino



should have more flavors and could change into another flavor (Pontecorvo, 1958). After that, the muon neutrino was detected from a pion decay at Brookhaven National Laboratory.

Then, the new aspect of the extraterrestrial high-energy neutrino experiment was proposed. The first neutrino from the sun, or solar neutrino, was detected (energy  $\sim 400$  keV to 18 MeV, see Figure 2.2) in 1968 (Davis, Harmer, and Hoffman, 1968). This experiment left one of the biggest questions about neutrino physics, called solar neutrino problems, when the number of neutrinos disappeared by two-thirds from the prediction. However, the problem is resolved by the explanation of neutrino oscillation when neutrino transforms its flavor into another type, and this was confirmed by the observation in the collaboration between Super-Kamiokande (Super-K) and Sudbury Neutrino Observatory (SNO) (Fukuda et al., 1998; Ahmad et al., 2002). At this time, only two flavors, electron- and muon neutrino, were found before the discovery of tau neutrino in 2000 (Kodama et al., 2001).

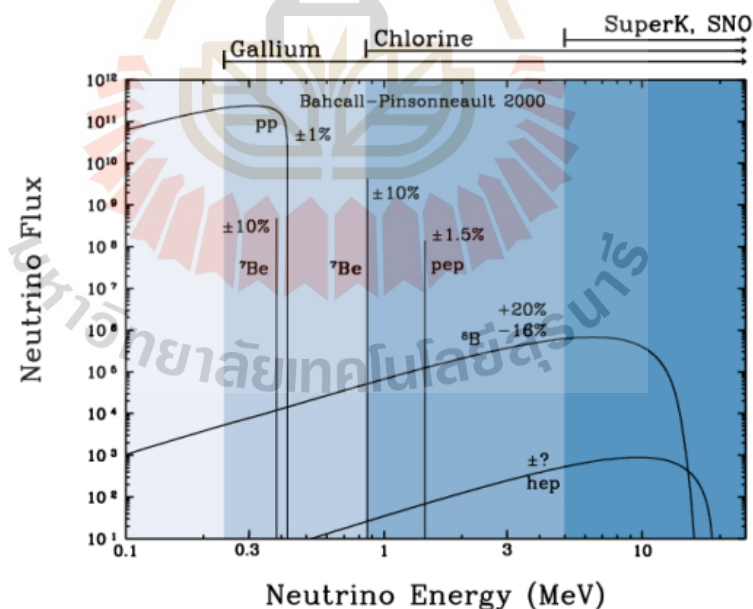


**Figure 2.2** The solar neutrino flux spectrum and energy (MeV). The color code is the efficient energy range of each experiment (Gallium, Chlorine, Super-K & SNO) (Bellerive, 2004).

In the golden period of the discovery, several detectors were planned or finished establishing and looked for the extraterrestrial source that could produce an abundance of neutrinos, for instance, atmospheric neutrino (Kajita, 2010), supernovae (Abbasi et al., 2009; Gerhardt et al., 2010; Bellerive, Klein, McDonald, Noble, and Poon, 2016; Yokoyama, 2017) and gamma-ray burst (GRB) (Paczynski and Xu, 1994; Kohri and Mineshige, 2002). Among of them, the remarkable source should belong to the gamma-ray burst (GRB) (Narayan et al., 1992) since they emit a great deal of energy around MeV. According to Table 2.1, a few neutrino detectors can also provide data collection from a detection in the MeV range. However, the origins of the GRBs are still under discussion. Therefore, this led us to detect more GRBs, and seek for the plausible candidate of the central engine of these GRBs.

**Table 2.1** List of neutrino detectors.

Neutrino detector	Location	Operation	Type of detector	Threshold energy
Davis Homestake (Chlorine)	Lead, South Dakota	1967– 1998	Radiochemical	814 keV
Super-Kamiokande (Super-K)	Kamioka, Japan	1996– present	Water Cherenkov	200 MeV
Sudbury Neutrino Observatory (SNO)	Creighton Mine, Ontario	1999– 2006	Water Cherenkov	3.5 MeV
IceCube	South Pole, Antarctica	2006– present	Water Cherenkov	≈10 GeV
Jiangmen Underground Neutrino Observatory (JUNO)	Kaiping, China	2014– present	Scintillation	1.8 MeV
Hyper-Kamiokande (Hyper-K)	Tokai and Kamioka, Japan	future	Water Cherenkov	200 MeV
LENA (CERN to Finland)	European	future	Scintillation	low

Recently, NDAFs around rotating black hole has become one of the most discussed topics since it possess high density and high temperature that satisfied the condition for driving GRB more than other accretion disk models (Popham et al., 1999; Narayan, Piran, and Kumar, 2001; Gu, Liu, and Lu, 2006; N. Kawanaka and Mineshige, 2007). This model will be discussed in detail in the next section.

## 2.2 NDAF black hole

Neutrino-dominated accretion flow, or NDAF, is the model of accretion disk around rotating (Kerr) black holes. This model has been proposed as a prominent candidate for the central engine of GRBs (Popham et al., 1999; Narayan et al., 2001; Kohri et al., 2005; W.-X. Chen and Beloborodov, 2007; Xue et al., 2013; Liu et al., 2017; Nagataki, 2018; B.-G. Chen et al., 2022; Wei and Liu, 2022). The notable point of NDAF disk is the neutrino cooling mechanism, which is capable to drive the GRB (Popham et al., 1999).

To search for NDAF, some suggested that this accretion disk origins from the black hole after merger scenarios, such as double neutron star binaries (NS-NS) (Eichler, Livio, Piran, and Schramm, 1989), neutron star-black hole binaries (NS-BH) (Paczynski, 1991), and the scenario of massive star collapsar (Woosley and Bloom, 2006). Therefore, NDAF in such scenarios may be the key to understanding how GRBs be formed, and how neutrinos originated in the universe. The background of NDAF and the application of neutrino physics will be discussed in the sub-section afterward, followed by the idea of neutrino oscillation.

### 2.2.1 History of NDAF model

The black hole is one of the mysterious cosmic subjects and still is the popular topic of discussion nowadays. However, we cannot directly observe the black hole due to the effect of gravity capturing the light or the photon inside. Therefore, the structure of the black hole can be obtained by using the theoretical model to describe the dynamics around the black hole and analyzing the data obtained by the indirect evidence. From the past, the accretion disk, a disklike flow of material, was proposed to be the component around the black hole. The accretion disk system has been discussed by various models such as Shakura-Sunyaev (SSD) (Shakura and Sunyaev,

1973), slim disk (Abramowicz, Czerny, Lasota, and Szuszkiewicz, 1988), and advection dominated accretion flow (ADAF) (Narayan and Yi, 1994).

Neutrino-dominated accretion flows (NDAFs) is widely known as the hyperaccretion disk model with high density and extremely high temperature in the inner region of the disk ( $\rho \sim 10^{10}-10^{13} \text{ g/cm}^3$ ,  $T \sim 10^{10}-10^{11} \text{ K}$ ) (Popham et al., 1999). This accretion disk can be formed in the merger scenarios, while energetic neutrinos and anti-neutrinos are emitted from the disk surface via the cooling mechanism. The Neutrino-antineutrino pair will become a part of the annihilation process, and result in a relativistic electron-positron pair dominated outflow which could powerfully drive the GRB (Jaroszynski, 1996). In the merger scenarios, the timescale of the evolution is of 1-100 s. The neutrino luminosity from this neutrino emission can approach  $10^{53}-10^{55} \text{ erg s}^{-1}$  (Popham et al., 1999; Xue et al., 2013). At the same time, another mechanism for driving GRB became an alternative study (e.g., the Blandford-Znajek mechanism), which also contribute to neutrino emission and neutrino annihilation (Blandford and Znajek, 1977; McKinney and Gammie, 2004; Hawley and Krolik, 2006; Norita Kawanaka, Piran, and Krolik, 2013; Norita Kawanaka and Masada, 2019; She, Liu, and Xue, 2022).

Up until now, after the first investigation of Popham, the study of NDAF model has become widened. One can consider the thin-disk approximation to the neutrino-cooled accretion disk around stellar-mass black holes and takes into account general relativistic effects with common parameter: mass accretion rates ( $\dot{M}$ ) about  $0.01-10 M_{\odot} \text{ s}^{-1}$ . Followed by the neutrino trapping effect, the bounded radius, that allows neutrino emission in specific region, occurs as a consequence of opacity (Di Matteo, Perna, and Narayan, 2002; Gu et al., 2006). The electron degeneracy parameter was introduced into the model, taking effect to the disk structure and neutrino emission (Kohri and Mineshige, 2002; Kohri et al., 2005).

From Figure 2.3, the characteristic of the neutrino on the disk are divided into separated regions according their mechanism (W.-X. Chen and Beloborodov, 2007) (I) Neutrino trapping region ( $r < r_{\text{trap}}$ ), preventing neutrino to be emitted from the surface, (II) Ignition region ( $r_{\text{trap}} < r < r_{\text{ign}}$ ), neutrino emission from cooling process dominates in this region, and (III) Neutrino opaque region ( $r = r_{\nu}$ ,  $r = r_{\bar{\nu}}$ ) where the

disk becomes opaque for antineutrino and neutrino, related to thermal distribution. Later, some presented the global solution for NDAF (Xue et al., 2013), considering the effect of electron degeneracy and mass fraction (Liu et al., 2017; Nagataki, 2018).

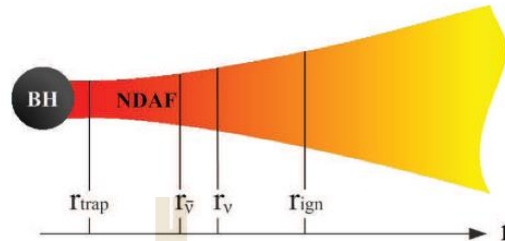


**Figure 2.3** Schematic picture of characteristic radii of NDAFs (Liu et al., 2017).

According to the observation of GRB, no direct evidence related to NDAFs black hole was discovered. Therefore, this will be a good sign to neutrino physics, if one can give a more accurate prediction for neutrino detected in merger scenarios, along with the observation of GRB. Later, ones can estimate MeV neutrinos detection from NDAF models, as one of the multi-messenger signals (Pan and Yuan, 2012; Liu, Gu, Kawanaka, and Li, 2015; Caballero, Zielinski, McLaughlin, and Surman, 2016; Liu, Zhang, et al., 2016; Wei and Liu, 2022). Based on Hyper-K detector, the total rate of neutrino and anti-neutrino, observed from GRB-related events at distances of 0.61 – 0.77 Mpc, was estimated to be about 0.10 – 0.25 events per century with an observed energy of  $10^{52}$  erg  $s^{-1}$  was estimated (Liu, Zhang, et al., 2016), see Table 2.2. However, this results in a concern that neutrinos can undergo oscillations around black hole as they propagate or traveling (Pontecorvo, 1958; Fukuda et al., 1998; Ahmad et al., 2002), when a number of neutrino from origin flavor can decrease in exchange for other flavors (estimated number in parenthesis in Table 4.2). Therefore, in this system containing a dense neutrino density, this effect of neutrino oscillation should be taking into account for a more realistic picture of NDAF model.

**Table 2.2** The detection rate and the optimistic detection rate of electron neutrino, for SN-related event, with the number of estimated rate including neutrino oscillation in the parenthesis (Liu, Zhang, et al., 2016).

Observatory	Detection rate	Optimistic detection rate
Hyper-K	~0.10–0.25 (0.03–0.08)	~1.0–3.0 (0.3–1.0)
JUNO	~0.095 (0.03)	~0.6 (0.2)
LENA	~0.095 (0.03)	~1.0 (0.3)

### 2.2.2 Neutrino oscillation on NDAF

Neutrino oscillation is the phenomenon that changes neutrino flavor from one to another (electron-, muon-, and tau neutrino). This phenomenon has the potential to alter the distribution of neutrino flavor over time. This effect has been investigated in the context of merger events, as the enhancement of nucleosynthesis in the outflow of the system (Malkus, Kneller, McLaughlin, and Surman, 2012; Frensel, Wu, Volpe, and Perego, 2017; Tian, Patwardhan, and Fuller, 2017; Wu and Tamborra, 2017; Becerra et al., 2018). In the NDAF model, the full impact of neutrino oscillations is still incomplete. This led to the investigation of neutrino oscillation inside the disk, which reported that the flux of electron neutrino transfer into other flavors and the total luminosity and annihilation luminosity dropped by a factor of 4–5 (Uribe et al., 2021). They also imply that the oscillation above the disk, which is still neglected in their work, should be considered at the same time.

In this work, we investigate the impact of neutrino oscillation on the annihilation luminosity above the disk within this NDAF framework and discuss the application in the further study of neutrino oscillation and GRB formation.



## CHAPTER III

### METHODOLOGY

This following section is from the manuscript, titled “Neutrino Oscillation Effects on the Luminosity of Neutrino-Dominated Accretion Flows Around Black Holes”. It was originally included there in section 2 and 3, the “NEUTRINO-DOMINATED ACCRETION FLOW MODEL” and “NEUTRINO OSCILLATION”. The manuscript is now under revision for publication in The Astrophysical Journal (ApJ) in 2024, article in press.

#### 3.1 Geometry and Model Assumptions

Firstly, we employ the NDAF model presented in (Popham et al., 1999). The accretion disk is assumed to be in steady-state where the accretion timescale is significantly shorter than the evolution timescale of mass accretion rate, and hence the disk can be characterized into distinctly separated regions (W.-X. Chen and Beloborodov, 2007), as illustrated in Figure 3.1 We adopt the thin-disk approximation, where  $H/r \leq 0.1 - 0.4$  ( $H$  is the half-thickness of the disk at radius  $r$  measured from the central black hole). The key parameters governing the hydrodynamic characteristics of the flow consist of the black hole spin ( $a$ ) and the mass accretion rate ( $\dot{M}$ ).

We set the outer radius of the disk at  $r_{\text{out}} = 500 r_g$  and the black hole mass  $M = 3 M_\odot$ ,  $1 r_g = 2 GM/c^2$ , where  $G = 6.67 \times 10^{-8} \text{ erg}^{-3} \text{ s}^{-1}$  is gravitational constant and  $c = 3 \times 10^{10} \text{ cm s}^{-1}$  is the speed of light) to ensure coverage of the emission radius (Xue et al., 2013). For the innermost region near the black hole, the advection effect dominates and the flows become optically thick. Consequently, photons and neutrinos/anti-neutrinos are trapped, precluding radiation emission. The trapping radius is chosen to be  $r_{\text{trp}} = 1.473 r_g$  which is an intermediate value and found in the cases of  $a \sim 0-0.99$  and  $\dot{M} \sim 0.01-10 M_\odot \text{ s}^{-1}$  (Xue et al., 2013). For comparison, we also look at the case when  $r_{\text{trp}} = 3 r_g$  in order to see the effect of variable  $r_{\text{trp}}$ . Within the ignition, or emission region ( $r_{\text{trp}} < r < r_{\text{ign}}$ ), the balancing between the viscous heating



and the cooling rate is satisfied so that neutrino emission switches on (W.-X. Chen and Beloborodov, 2007; Zalamea and Beloborodov, 2011). Under this setup, the neutrino and anti-neutrino emissions from the cooling process within the ignition region,  $r_{\text{trp}} < r < r_{\text{ign}}$ , can be calculated. Typically, the emission region extends largely to cover the area where neutrons and protons dominate the disk before transitioning into a region dominated by heavy atoms through the nucleosynthesis in the outermost region (Meyer, 1994; Xue et al., 2013; Janiuk, 2014; She et al., 2022), so we assume  $r_{\text{ign}} = r_{\text{out}}$ . Subsequently, the neutrinos and anti-neutrinos emitted from the surface of the disk propagate through space covering distances  $d_k$  and  $d_{k'}$  respectively (as depicted by arrows in Figure 3.1 before they annihilate. The annihilation luminosity above the disk, denoted as  $l_{\nu\bar{\nu}}$ , are computed for each point. Then, we compute the obtained total luminosity, comparing between the cases with and without the effects of the neutrino oscillation, as explained in the following sections.

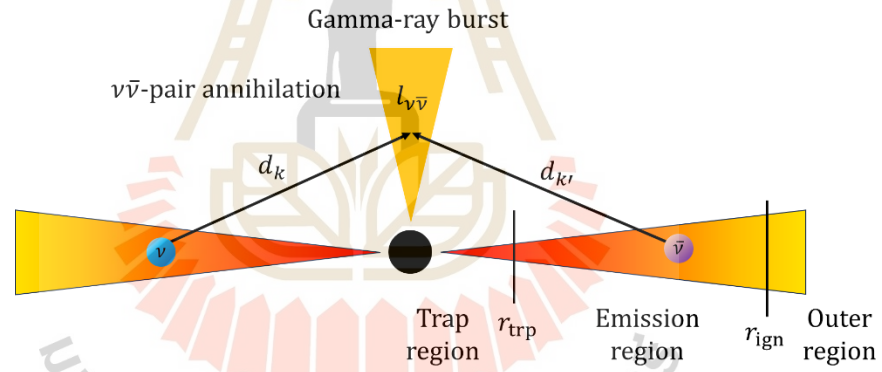


**Figure 3.1** Schematic of a simplified neutrino-cooled accretion disk model (not to scale). The disk regions are separated into the trapping region ( $r < r_{\text{trp}}$ ), emission region ( $r_{\text{trp}} < r < r_{\text{ign}}$ ), and outer region ( $r > r_{\text{ign}}$ ). Neutrino  $\nu$  and anti-neutrino  $\bar{\nu}$  emitted from the surface of the disk will propagate through space with distances  $d_k$  and  $d_{k'}$ , respectively, and will annihilate above the disk yielding annihilation luminosity  $l_{\nu\bar{\nu}}$  at specific points.

### 3.2 Disk Temperature and Density Profile

The temperature  $T$  and the density  $\rho$  of the accretion disk can be determined by numerically solving the equation of state of the disk that involves considering continuity equations and balancing the cooling mechanism with various thermodynamic properties such as internal energy and pressure (Popham et al., 1999; Kohri et al., 2005; W.-X. Chen and Beloborodov, 2007; Xue et al., 2013; Liu et al., 2017). Additionally, the temperature and density profiles depend on the choice of model assumptions. The inclusion of chemical processes within the flow such as neutrino trapping effects (Di Matteo et al., 2002), electron degeneracy in neutrino emission (Kohri et al., 2005), and photodisintegration for heavy nuclei from nuclear statistical equilibrium (NSE) (Seitenzahl et al., 2008), all contribute to the cooling mechanism and result in changes to the thermodynamic properties of the disk. The relativistic calculation of the hydrodynamic properties of the NDAF, incorporating detailed neutrino physics, the balance of chemical potentials, photodisintegration, and nuclear statistical equilibrium, was conducted by (Xue et al., 2013). Later, (Liu, Zhang, et al., 2016) derived solutions for the disk temperature, which depend on key parameters including  $a$  and  $\dot{M}$ .

In this work, we employ the empirical solution from (Liu, Zhang, et al., 2016) to introduce the temperature profile of the disk:

$$\log T (K) = 11.09 + 0.10a + 0.20 \log \dot{m} - 0.59 \log R, \quad [1]$$

where  $\dot{m} = \dot{M}/(M_{\odot} s^{-1})$  and  $R = r/r_g$ . To determine the density profile of the disk, we consider the charge-neutrality constraints for the neutral disk (Liu, Gu, Xue, and Lu, 2007). Specifically, the number density of protons  $n_p$  must equal to the number density of electrons  $n_{e^-}$  excluding the positron pairs  $n_{e^+}$ , i.e.

$$n_p = \frac{\rho Y_e}{m_p} = n_{e^-} - n_{e^+}, \quad [2]$$

where  $\rho$  and  $m_p$  are the density and mass of the proton.  $Y_e$  is the proton-to-nucleon ratio (related to proton-neutron number density). In this case, we assume that the matter is completely dissociated where nuclear statistical equilibrium (NSE) is neglected (Meyer, 1994) and thus the atomic mass fraction can also be neglected

(Kohri et al., 2005). Then, one can obtain  $Y_e$  in terms of the proton number density  $n_p$  and the neutron number density  $n_n$  as

$$Y_e = \frac{n_p}{n_p + n_n}, \quad [3]$$

In the equilibrium radiation reaction  $e^+ + e^- \leftrightarrow \gamma + \gamma$ , the chemical potential for photons is zero. It follows that  $\mu_{e^-} + \mu_{e^+} = 0$  and we denote the electron chemical potential  $\mu_{e^-} = \mu_e$ . The number density of electron/positron is given by the Fermi-Dirac integral,

$$n_{e^\pm} = \frac{1}{\hbar^3 \pi^2} \int_0^\infty \frac{1}{e^{(\sqrt{p^2 c^2 + m_e^2 c^4} \mp \mu_e)/k_B T} + 1} p^2 dp, \quad [4]$$

In perfect equilibrium, the precise calculation of the electron chemical potential is determined by the reaction between protons and neutrons (Kohri et al., 2005),

$$\left(\frac{n}{p}\right)_{eq} = \exp\left(-\frac{Q}{k_B T} + \eta_e\right), \quad [5]$$

where  $\eta_e = \mu_e/k_B T$  is the degeneracy of electrons and  $Q = (m_n - m_p)c^2 \simeq 1.29$  MeV is the rest-mass difference between a neutrino and a proton. For the conditions in Equations [3] and [5], we simplify the thermodynamic quantities by fixing the number of neutrino degeneracy parameter  $\eta_e$  for all disk emission radii with the boundary condition  $Y_e = 0.5$  at the outer radius (Liu et al., 2017). The number density of each particle:  $n_{e^-}$ ,  $n_{e^+}$ ,  $n_p$ ,  $n_n$ , the electron fraction  $Y_e$ , and the matter density  $\rho$  can be estimated in the simplest way instead of solving complicated non-linear equations. The obtained parameters  $T$  and  $\rho$  are then used to determine the cooling rate and the luminosity of the disk.

### 3.3 Cooling Processes and Luminosity

Different from other accretion disk models, NDAF has the cooling mechanism that provides neutrino emission dominating the disk. The cooling rate due to the neutrino loss in the cooling process is given by (Di Matteo et al., 2002; Kohri et al., 2005; Liu et al., 2007),

$$Q_v = \sum_i Q_{v_i} = \sum_i \frac{(7/8)\sigma T^4}{(3/4)[\tau_{v_i/2+1/\sqrt{3}+1/(3\tau_{a,v_i})}]}, \quad [6]$$

where  $\sigma$  is the Stephan-Boltzmann constant. The subscript  $i$  runs for three flavors of neutrinos: electron neutrino ( $\nu_e$ ), muon neutrino ( $\nu_\mu$ ), and tau neutrino ( $\nu_\tau$ ). The neutrino optical depth  $\tau_\nu$  is defined by

$$\tau_{\nu_i} = \tau_{s,\nu_i} + \tau_{a,\nu_i}, \quad [7]$$

where  $\tau_{s,\nu_i}$  and  $\tau_{a,\nu_i}$  represent the neutrino optical depths resulting from scattering and absorption, respectively. These quantities can be expressed as

$$\tau_{s,\nu_i} = H(\sigma_{e,\nu_i} n_e + \sum_j \sigma_{j,\nu_i} n_j), \quad [8]$$

$$\tau_{a,\nu_i} = \frac{q_{\nu_i} H}{4(7/8)\sigma T^4}, \quad [9]$$

Here,  $\sigma_{e,\nu_i}$  and  $\sigma_{j,\nu_i}$  denote the cross sections of electron and nucleons, respectively.  $n_e$  and  $n_j$  ( $j = 1, 2, 3, \dots$ ) are the number densities of electrons and nucleons, respectively. Note that  $n_1$  and  $n_2$  are the number density of free protons and free neutrons.  $q_{\nu_i}$  is the total neutrino cooling rate (per unit volume) encompassing four main cooling processes: Urca process, electron-positron annihilation, Bremsstrahlung, and Plasmon decay. Further details regarding the cross-section calculations are provided in Appendix A.

The neutrino luminosity can be obtained by integrating the neutrino cooling rate  $Q_\nu$  along one-dimensional radius,

$$L_\nu = 4\pi \int_{r_{in}}^{r_{out}} Q_\nu r' dr', \quad [10]$$

where the inner radius for the neutrino emission is set to be  $r_{in} = r_{trp} = 1.473 r_g$ , while the outer radius is set to be  $r_{out} = r_{ign} = 500 r_g$ . The value  $4\pi$  refers to the radiation emitted from all directions in spherical symmetry.

### 3.4 Annihilation Luminosity

To calculate the neutrino annihilation luminosity from the NDAF model, we follow the approach outlined in (Popham et al., 1999; Ruffert and Janka, 1999; Rosswog, Ramirez-Ruiz, and Davies, 2003; Liu et al., 2007; Norita Kawanaka and Masada, 2019).

We create a grid of cells for the disk in the equatorial plane by dividing the disk logarithmically into 400 bins. A cell  $k(k')$  on the disk has its mean neutrino (anti-neutrino) energy  $\epsilon_{\nu_i}^k(\epsilon_{\bar{\nu}_i}^{k'})$  and differential neutrino luminosity  $l_{\nu_i}^k(l_{\bar{\nu}_i}^{k'})$  for each

neutrino (anti-neutrino) flavor  $\nu_i$  ( $\bar{\nu}_i$ ). We calculate  $l_{\nu_i}^k = 4\pi Q_{\nu_i} r_k \Delta r_k$  by integrating the cooling rate (Equation [6]) of each flavor of neutrino  $Q_{\nu_i}$  separately over the surface of cell  $k$  before summing the luminosity over the entire disk surface. Similarly, we calculate  $l_{\bar{\nu}_i}^{k'}$  for the anti-neutrino. Note that  $r_k$  is the distance from the central black hole to the center of the cell  $k$ , and  $\Delta r_k$  is the radial size of cell  $k$ . Let us denote  $d_k$  as the distance traveled by neutrinos emitted from a specific cell  $k$  on the disk to the annihilation point, and  $d_{k'}$  as the corresponding distance for anti-neutrinos emitted from another cell  $k'$ . The neutrino annihilation luminosity at each specific point above the disk is given by summing the contributions of neutrino and anti-neutrino radiation from all pairs of disk cells (Popham et al., 1999),

$$l_{\nu\bar{\nu}} = \sum_i A_{1,i} \sum_k \frac{l_{\nu_i}^k}{d_k^2} \sum_{k'} \frac{l_{\bar{\nu}_i}^{k'}}{d_{k'}^2} (\epsilon_{\nu_i}^k + \epsilon_{\bar{\nu}_i}^{k'}) (1 - \cos \theta_{kk'})^2, \quad [11]$$

$$+ \sum_i A_{2,i} \sum_k \frac{l_{\nu_i}^k}{d_k^2} \sum_{k'} \frac{l_{\bar{\nu}_i}^{k'}}{d_{k'}^2} \frac{\epsilon_{\nu_i}^k + \epsilon_{\bar{\nu}_i}^{k'}}{\epsilon_{\nu_i}^k \epsilon_{\bar{\nu}_i}^{k'}} (1 - \cos \theta_{kk'}), \quad [12]$$

where  $A_{1,i} = (1/12\pi^2)[\sigma_0/c(m_e c^2)^2] [(C_{V,\nu_i} - C_{A,\nu_i})^2 + (C_{V,\nu_i} + C_{A,\nu_i})^2]$ ,  $A_{2,i} = (1/6\pi^2)[\sigma_0/c][2C_{V,\nu_i}^2 - C_{A,\nu_i}^2]$ , and  $\theta_{kk'}$  is the angle at which neutrinos from cell  $k$  encounter anti-neutrinos from another cell  $k'$ . Here,  $d$  and  $\epsilon$  are in cm and erg units, respectively. All constant values are shown in Appendix A.

The total neutrino annihilation luminosity,  $L_{\nu\bar{\nu}}$ , is obtained by integrating over the whole space outside the black hole and the disk (Xue et al., 2013),

$$L_{\nu\bar{\nu}} = 4\pi \int_H^\infty \int_{r_{\text{in}}}^\infty l_{\nu\bar{\nu}}(r', z') r' dr' dz', \quad [13]$$

where  $r_{\text{in}} = r_{\text{trp}}$ .

### 3.5 Neutrino Oscillation

In the calculation of neutrino oscillation effects on the annihilation luminosity, three neutrino flavor eigenstates ( $\nu_e, \nu_\mu, \nu_\tau$ ) and their antiparticles are initially produced in the cooling mechanism via weak interaction. We assume that they are emitted from the disk simultaneously. Subsequently, they propagate out of the disk with their mass eigenstates:

$$|\nu_i\rangle = \sum_{\alpha=1,2,3} U_{i\alpha} |\nu_\alpha\rangle, \quad [14]$$

where  $U_{i\alpha}$  is the Pontecorvo-Maki-Nakagawa-Sakata (PMNS) matrix, a unitary matrix describing neutrino mixing (see Appendix B for full details). These neutrinos and anti-neutrinos oscillate until they reach the specific points above the disk and annihilate. The traveling distance of neutrino and anti-neutrino are approximated by  $d_k$  and  $d_{k'}$ , which play a role in determining neutrino oscillation behavior as they traverse through space before annihilating. For simplicity, we further assume that the three neutrino (anti-neutrino) flavors from the same cell  $k$  have neither self-interaction nor interaction with each other, and the energies carried by these particles are the same at the annihilation point. Considering that most of the annihilation points are far enough from the black hole and assuming there is no outflow from the disk in the vertical direction, then we could treat the oscillation in the vacuum limit. The probability of the flavor transition from neutrino  $i$  ( $\nu_i$ ) to neutrino  $j$  ( $\nu_j$ ) ( $P_{\nu_\alpha \rightarrow \nu_\beta}$ ) is given by

$$P_{\nu_i \rightarrow \nu_j} = -4 \sum_{\alpha > \beta} (U_{i\alpha}^* U_{j\alpha} U_{i\beta} U_{j\beta}^*) \sin^2 \left( 1.27 \Delta m_{\alpha\beta}^2 \frac{d_k(\text{km})}{\epsilon_{\nu_i}^k(\text{GeV})} \right) + 2 \sum_{\alpha > \beta} (U_{i\alpha}^* U_{j\alpha} U_{i\beta} U_{j\beta}^*) \sin^2 \left( 1.27 \Delta m_{\alpha\beta}^2 \frac{d_k(\text{km})}{\epsilon_{\nu_i}^k(\text{GeV})} \right), \quad [15]$$

where  $\Delta m_{\alpha\beta}^2 = m_\alpha^2 - m_\beta^2$  is the neutrino mass-squared difference. The values adopted for the normal mass hierarchy, obtained from the global fit of neutrino oscillation parameters provided by the Particle Data Group (PDG) (Workman et al., 2022), are  $\Delta m_{21}^2 = 7.53 \times 10^{-5}$ ,  $\Delta m_{32}^2 = 2.453 \times 10^{-3}$ , and  $\Delta m_{31}^2 = \Delta m_{21}^2 + \Delta m_{32}^2$ .

In the Standard Model, the violation of charge conjugation parity symmetry (CP-violation) is considered to be a significant factor in distinguishing the flavor transition of neutrinos from anti-neutrinos (Nunokawa, Parke, and Valle, 2008; T2K Collaboration, 2020). In this work, we compare two cases where the CP-violating phase ( $\delta_{CP}$ ) in the PMNS matrix is varied to be  $0^\circ$  and  $245^\circ$ . The plausible value of  $\delta_{CP} = 245^\circ$  is based on the recent global fit of the average CP-violating phase measured in atmospheric and accelerator experiments: T2K, NOVA, and SKAM (Workman et al., 2022).  $\delta_{CP} = 245^\circ$  introduces an extra phase term resulting in the different transition probability between  $\nu_i \rightarrow \nu_j$  and  $\bar{\nu}_i \rightarrow \bar{\nu}_j$  (Nunokawa et al., 2008) as given by

$$P_{\bar{\nu}_i \rightarrow \bar{\nu}_j} = P_{\nu_i \rightarrow \nu_j} - 4 \sum_{\alpha > \beta} (U_{i\alpha}^* U_{j\alpha} U_{i\beta} U_{j\beta}^*) \sin \left( 2.54 \Delta m_{\alpha\beta}^2 \frac{d_k}{\epsilon_{\nu_i}^k} \right). \quad [16]$$

The transition probabilities (Equations [14]–[15]) are utilized to account for the change in the total number of neutrinos and anti-neutrinos of the initial flavor before the neutrino annihilation luminosity (Equation [11]) is calculated. We assume that the luminosities of flavor  $i$  of neutrino and anti-neutrino at the annihilation point from those cells are given by  $P_{\nu_i \rightarrow \nu_i} \cdot l_{\nu_i}^k$  and  $P_{\bar{\nu}_i \rightarrow \bar{\nu}_i} \cdot l_{\bar{\nu}_i}^{k'}$ . The rest of the particles turning into other flavors could transfer their initial energies into other annihilation processes corresponding to their final flavor states with luminosities  $P_{\nu_i \rightarrow \nu_j} \cdot l_{\nu_i}^k$  and  $P_{\bar{\nu}_i \rightarrow \bar{\nu}_j} \cdot l_{\bar{\nu}_i}^{k'}$ .





## CHAPTER IV

### RESULTS

This following section is from the manuscript, titled “Neutrino Oscillation Effects on the Luminosity of Neutrino-Dominated Accretion Flows Around Black Holes”. It was originally included there in section 4, the “RESULTS”. The manuscript is now under revision for publication in The Astrophysical Journal (ApJ) in 2024, article in press.

Firstly, we calculate various thermodynamic quantities, including temperature (Equation [1]), matter density (Equation [3]), neutrino and anti-neutrino cooling rates (Equation [6]), and luminosity (Equation [10]) for different mass accretion rates  $\dot{m} = 0.1, 1, 10$  and black hole spins  $a = 0, 0.5, 0.99$ . Figure 4.1 shows the temperature profiles of the accretion disk when the black hole mass and the half-thickness of the disk are fixed, as an example, at  $M = 3 M_{\odot}$  and  $H/r = 0.1$ .

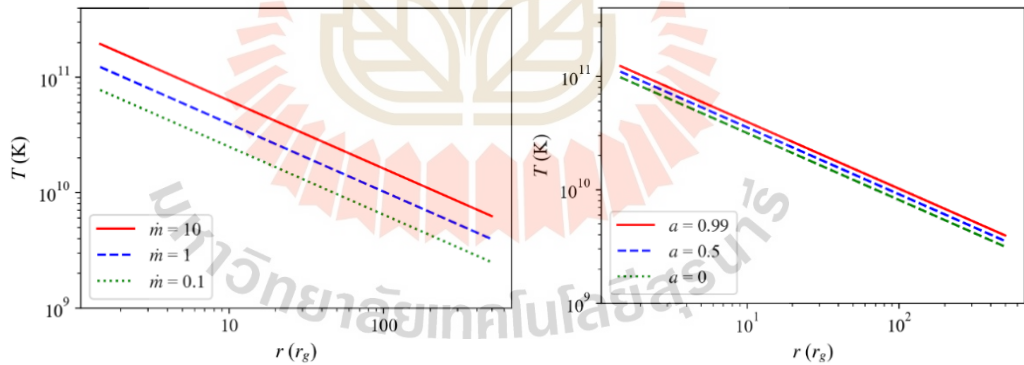


**Figure 4.1** Disk temperature profiles for  $a = 0.99$  (left) when  $\dot{m} = 0.1, 1, 10$  (dotted, dashed, and solid lines respectively), and for  $\dot{m} = 1$  (right) when  $a = 0, 0.5, 0.99$  (dotted, dashed, and solid lines, respectively).

As previously mentioned, our temperature profile is employed from the empirical solution derived by (Liu, Zhang, et al., 2016), allowing us to infer the effects of  $\dot{m}$  and  $a$  on  $T$  from the coefficients of Equation [1]. As expected, higher temperature is observed in the cases of higher  $\dot{m}$  and  $a$ , and the change in the temperature is more

sensitive to variations in  $\dot{m}$  than in  $a$ . Additionally, the disk temperature increases towards the innermost region closer to the central black hole.

Figure 4.2 illustrates how the neutrino cooling rate varies across the disk. The cooling rate scales with the disk temperature and significantly depends on the optical depth  $\tau$ , which links to the number density of electrons, protons, and neutrons. It is evident that the cooling rate also increases with  $\dot{m}$  and  $a$ . Furthermore, in the inner region  $r \lesssim 10 r_g$ , the cooling rate for anti-neutrinos exceeds that of neutrinos. This is due to the dominance of free nucleons in the dissociated matter, with the number densities of heavier nuclei being neglected. Therefore, the neutrino emission from cooling mechanism only depends on free nucleons. According to Equation [5], the fixed  $\eta_e$  results in the domination of neutrons in the region near a black hole, and hence the cooling process produces more anti-neutrino than neutrino in this region.

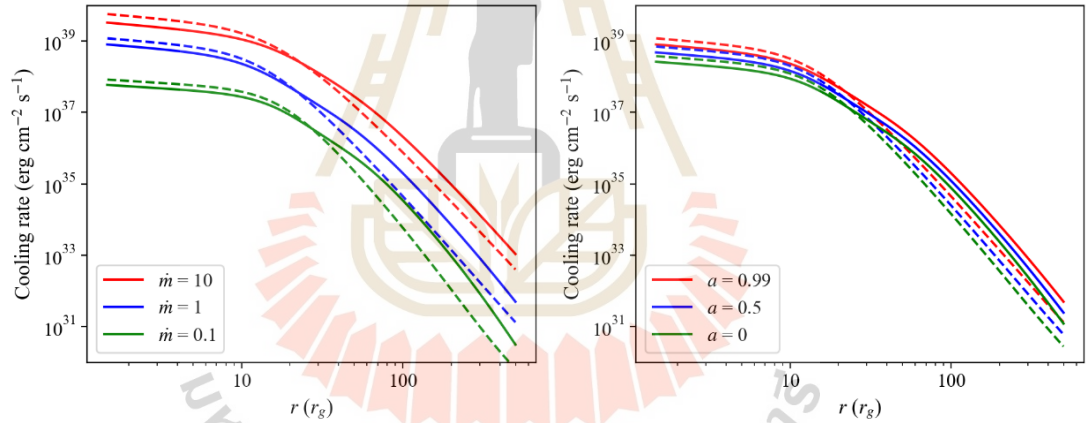


**Figure 4.2** Radial profiles of neutrino cooling rate  $Q_{\nu} = \sum_i Q_{\nu_i}$  (solid line) and anti-neutrino cooling rate  $Q_{\bar{\nu}} = \sum_i Q_{\bar{\nu}_i}$  (dashed line) as a function of  $r$  for  $a = 0.99$  (left), when  $\dot{m} = 0.1, 1, 10$  (green, blue, and red color respectively), and for  $\dot{m} = 1$  (right), when  $a = 0, 0.5, 0.99$  (green, blue, and red color respectively).

Figure 4.3 shows the corresponding neutrino and anti-neutrino luminosities obtained by integrating the cooling rate over the disk emission radius. The highest neutrino and anti-neutrino luminosity is obtained from the disk at  $r \sim 10 r_g$ , with the maximum luminosity reaching approximately  $10^{53} \text{ erg s}^{-1}$  for high accretion rate case ( $\dot{m} = 10$ ). At  $r \gtrsim 10 r_g$ , the luminosity decreases, consistent with the trend observed in the cooling rate. However, we can see that the luminosity drops at the innermost

region where  $r \lesssim 10 r_g$ . This is because, while the cooling rate at  $r \lesssim 10 r_g$  is high (Figure 4.2), the responding area is small, so the obtained luminosity over this area becomes small.

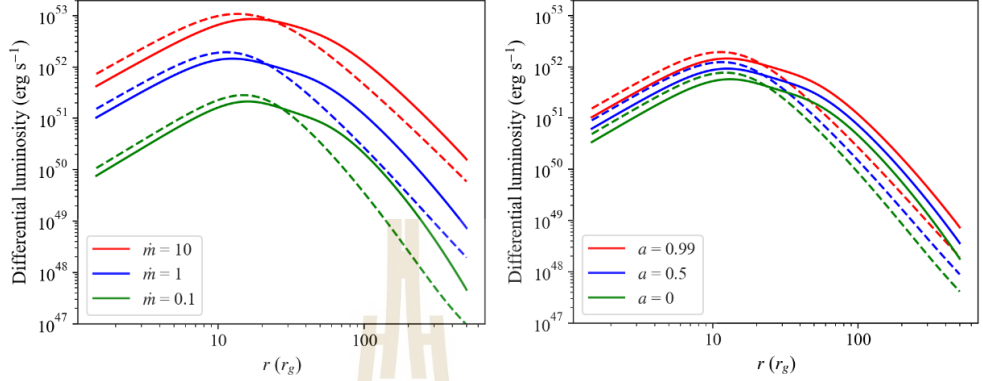


**Figure 4.3** Radial profiles of the neutrino luminosity (solid lines) and anti-neutrino luminosity (dashed lines) as a continuous function of  $r$  for  $a = 0.99$  (left), when  $\dot{m} = 0.1, 1, 10$  (green, blue, and red color respectively), and for  $\dot{m} = 1$  (right), when  $a = 0, 0.5, 0.99$  (green, blue, and red color respectively).

The corresponding annihilation luminosity for all neutrino (anti-neutrino) flavors is shown in Table 4.1. We compare the results with and without the effect of the neutrino oscillation. Here, the CP-violating phase is set to be  $\delta CP = 0^\circ$ . For all cases, the flavor transition in the vacuum results in a reduction of muon neutrino annihilation luminosity around 4–8%. On the contrary, the electron neutrino luminosity increases by 12–34%, as  $a$  and  $\dot{m}$  increase, while tau neutrino luminosity increases by 14–34% as  $a$  and  $\dot{m}$  decrease. The reason is that the magnitude of the annihilation luminosity drops with  $d^4$  (See Equation [11]) when the mean energy of neutrino (anti-neutrino) is around MeV. According to Equation [14], at a short distance above the black hole, a number of energetic  $\nu_\mu$  are transformed with higher probability into  $\nu_e$  in higher  $a$  and  $\dot{m}$  region and into  $\nu_\tau$  in lower  $a$  and  $\dot{m}$  region. In addition, the coupling rate of  $\nu_e$  is higher than that of other neutrinos, leading to a higher total annihilation luminosity.

**Table 4.1** Annihilation luminosity of neutrinos dependent on the spin parameter  $a$  and the unitless mass accretion rate  $\dot{m}$ . Results are presented separately for each flavor denoted with the subscripts  $e$ , and  $x$  ( $\mu$  and  $\tau$ ) for the parameters of electron-, and muon- and tau neutrino, respectively. We compare the cases of the total annihilation luminosity obtained when neutrino oscillation is neglected ( $L_{\nu\bar{\nu}}$ ) and when it is taken into account ( $L_{\nu\bar{\nu}}^{osc,0}$ ). Their relative difference defined as  $\Delta L_{\nu\bar{\nu}}^{osc}/L_{\nu\bar{\nu}} = (L_{\nu\bar{\nu}}^{osc,0} - L_{\nu\bar{\nu}})/L_{\nu\bar{\nu}}$  is also presented in the last column.

$a$	$\dot{m}$	$L_{\nu_e\bar{\nu}_e}$ (erg s <sup>-1</sup> )	$L_{\nu_x\bar{\nu}_x}$ (erg s <sup>-1</sup> )	$L_{\nu_e\bar{\nu}_e}^{osc,0}$ (erg s <sup>-1</sup> )	$L_{\nu_x\bar{\nu}_x}^{osc,0}$ (erg s <sup>-1</sup> )	$L_{\nu\bar{\nu}}^{osc,0}/L_{\nu\bar{\nu}}$
0	0.1	1.31×10 <sup>50</sup>	1.26×10 <sup>50</sup>	1.77×10 <sup>50</sup>	1.35×10 <sup>50</sup>	0.208
0	1	1.52×10 <sup>52</sup>	1.81×10 <sup>52</sup>	1.86×10 <sup>52</sup>	1.96×10 <sup>52</sup>	0.148
0	10	1.05×10 <sup>54</sup>	1.28×10 <sup>54</sup>	1.20×10 <sup>54</sup>	1.47×10 <sup>54</sup>	0.149
0.5	0.1	4.49×10 <sup>50</sup>	4.70×10 <sup>50</sup>	5.98×10 <sup>50</sup>	4.93×10 <sup>50</sup>	0.188
0.5	1	4.62×10 <sup>52</sup>	5.60×10 <sup>52</sup>	5.51×10 <sup>52</sup>	6.18×10 <sup>52</sup>	0.142
0.5	10	2.79×10 <sup>54</sup>	3.36×10 <sup>54</sup>	3.17×10 <sup>54</sup>	3.83×10 <sup>54</sup>	0.137
0.99	0.1	1.46×10 <sup>51</sup>	1.61×10 <sup>51</sup>	1.89×10 <sup>51</sup>	1.68×10 <sup>51</sup>	0.160
0.99	1	1.38×10 <sup>53</sup>	1.62×10 <sup>53</sup>	1.56×10 <sup>53</sup>	1.81×10 <sup>53</sup>	0.146
0.99	10	7.03×10 <sup>54</sup>	8.42×10 <sup>54</sup>	7.90×10 <sup>54</sup>	9.50×10 <sup>54</sup>	0.127

A global picture of the relative difference of the total annihilation luminosity with and without neutrino oscillation when  $\delta CP = 0^\circ$  is illustrated in Figure 4.4. Neutrino oscillation tends to increase the annihilation luminosity by a factor of  $\sim 0.127$ – $0.208$ . The difference is more pronounced for lower values of  $a$  and  $\dot{m}$ . Since the oscillation term depends on the ratio of the propagating distance per energy  $d/\epsilon$ , an increase of  $a$  and  $\dot{m}$  will enhance the mean energies from local areas of the disk and broaden the oscillation pattern at the same propagating distance, hence reduce the flavor transition.

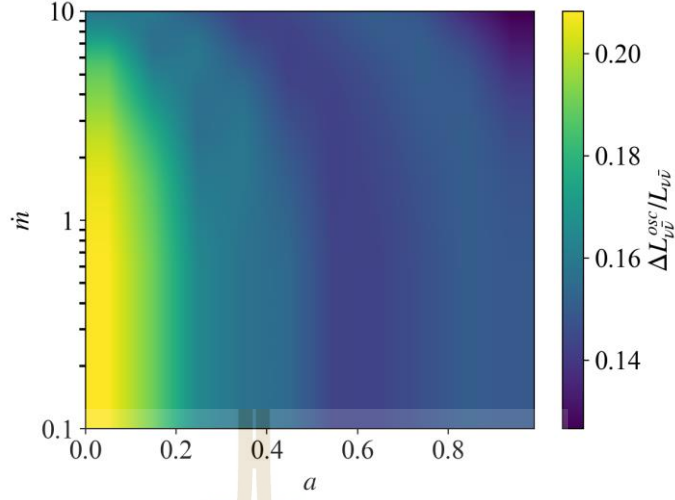


**Figure 4.4** Relative annihilation luminosity difference  $\Delta L_{\nu\bar{\nu}}^{osc}/L_{\nu\bar{\nu}}$  varying with  $a$  and  $m$ . Note that we define  $\Delta L_{\nu\bar{\nu}}^{osc}/L_{\nu\bar{\nu}} = (L_{\nu\bar{\nu}}^{osc,0} - L_{\nu\bar{\nu}})/L_{\nu\bar{\nu}}$  as the relative difference of the total annihilation luminosity between the cases when the effect of neutrino oscillation is included ( $L_{\nu\bar{\nu}}^{osc,0}$ ) and excluded ( $L_{\nu\bar{\nu}}$ ). The CP-violating phase is  $\delta CP = 0$ .

Finally, we investigate the effect of the CP-violating phase by introducing the recent plausible value of  $\delta CP = 245^\circ$ . We calculate the relative difference of the annihilation luminosity  $\Delta L_{\nu\bar{\nu}}^{CP}/L_{\nu\bar{\nu}}^{osc,0} = (L_{\nu\bar{\nu}}^{osc,245} - L_{\nu\bar{\nu}}^{osc,0})/L_{\nu\bar{\nu}}^{osc,0}$ , where  $L_{\nu\bar{\nu}}^{osc,245}$  and  $L_{\nu\bar{\nu}}^{osc,0}$  represent the annihilation luminosity for  $\delta CP = 245^\circ$  and  $\delta CP = 0^\circ$ , respectively. The result is shown in Figure 4.5. Note that, according to our definition of  $\Delta L_{\nu\bar{\nu}}^{CP}/L_{\nu\bar{\nu}}^{osc,0}$ , the plus (minus) value means that the annihilation luminosity in the cases of  $\delta CP = 245^\circ$  is more (less) than when  $\delta CP = 0^\circ$ . As  $a$  and  $m$  vary, the oscillation pattern changes in two ways simultaneously. Firstly, the addition of CP-violating phase can shift the oscillation pattern when the imaginary part in Equation [15] is non-negligible. Secondly, the energies raised by increasing  $a$  and  $m$  can slow down the flavor transformation, thereby broadening the oscillation pattern.

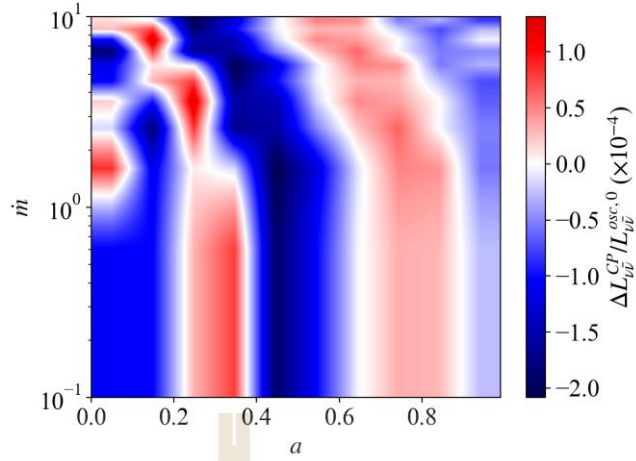


**Figure 4.5** Relative annihilation luminosity difference  $\Delta L_{\nu\bar{\nu}}^{CP}/L_{\nu\bar{\nu}}^{osc,0} = (L_{\nu\bar{\nu}}^{osc,245} - L_{\nu\bar{\nu}}^{osc,0})/L_{\nu\bar{\nu}}^{osc,0}$  varying with  $a$  and  $\dot{m}$ . This figure highlights the effects of the CP-violating phase on the total annihilation luminosity where  $L_{\nu\bar{\nu}}^{osc,245}$  and  $L_{\nu\bar{\nu}}^{osc,0}$  refer to the cases when  $\delta CP = 245^\circ$  and  $\delta CP = 0^\circ$ , respectively. Plus (red) and minus (blue) values indicate the case when  $L_{\nu\bar{\nu}}^{osc,245} > L_{\nu\bar{\nu}}^{osc,0}$  and  $L_{\nu\bar{\nu}}^{osc,245} < L_{\nu\bar{\nu}}^{osc,0}$ , respectively.

Last but not least, we derive equations of  $L_{\nu\bar{\nu}}$ ,  $L_{\nu\bar{\nu}}^{osc,0}$ , and  $L_{\nu\bar{\nu}}^{osc,245}$  as functions of  $a$  and  $\dot{m}$  from our model using linear regression fitting. The obtained relations are

$$\log L_{\nu\bar{\nu}} = 52.472 + 0.957a + 1.914 \log \dot{m}, \quad [17]$$

$$\log L_{\nu\bar{\nu}}^{osc,0} = 52.537 + 0.952a + 1.907 \log \dot{m}, \quad [18]$$

$$\log L_{\nu\bar{\nu}}^{osc,245} = 52.529 + 0.951a + 1.906 \log \dot{m}. \quad [19]$$

This allows for a direct comparison between our  $L_{\nu\bar{\nu}}$  and those derived by other authors, such as (Fryer, Woosley, Herant, and Davies, 1999), (Xue et al., 2013), and (Liu, Xue, Zhao, Zhang, and Zhang, 2016), as presented in the black lines in Figure 4.6. Notably, these authors did not consider the effect of neutrino oscillation in their calculations. The trend of increasing  $L_{\nu\bar{\nu}}$  with  $a$  and  $\dot{m}$  is consistent, but the obtained amplitudes of  $L_{\nu\bar{\nu}}$  are different. Additionally, in Figure 4.6 we also show in red lines the derived relation for  $L_{\nu\bar{\nu}}^{osc,0}$ , corresponding to the case where neutrino oscillation with  $\delta CP = 0^\circ$  is taken into account. Interestingly, the impact of neutrino oscillation on the annihilation luminosity appears to be less significant compared to the variations resulting from different assumptions made in the NDAF models used among different authors.

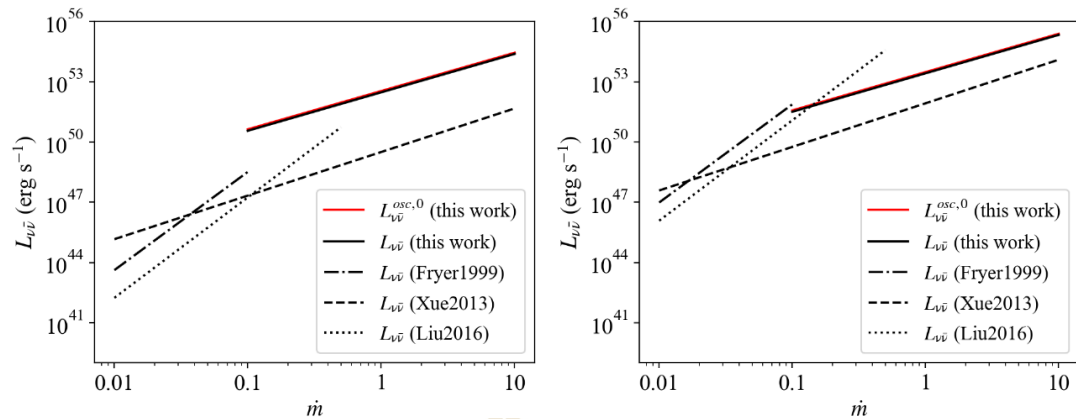


**Figure 4.6** Comparison of results in the annihilation luminosity with neutrino oscillation  $L_{\nu\bar{\nu}}^{osc,0}$  for  $\delta CP = 0^\circ$  (red solid line), and without neutrino oscillation  $L_{\nu\bar{\nu}}$  (black solid line), based on the Equations [16]–[17] derived from the fits with  $a$  and  $\dot{m}$  using linear regression method. The panels show the different fits between  $a = 0$  (left), and  $a = 0.99$  (right). Note that the annihilation luminosity for  $\delta CP = 0^\circ$  is not much different from  $\delta CP = 245^\circ$ . Results are compared with the fit obtained by (Fryer et al., 1999) (dash-dotted line), (Xue et al., 2013) (dashed line), and (Liu, Xue, et al., 2016) (dotted line).



## CHAPTER V

### DISCUSSION AND CONCLUSION

This following section is from the manuscript, titled “Neutrino Oscillation Effects on the Luminosity of Neutrino-Dominated Accretion Flows Around Black Holes”. It was originally included there in section 5, the “DISCUSSION AND CONCLUSION”. The manuscript is now under revision for publication in The Astrophysical Journal (ApJ) in 2024, article in press.

In this work, we investigate the neutrino/anti-neutrino luminosity and annihilation luminosity from the NDAF system by focusing on the effects of the neutrino oscillation above the accretion disk. The disk is assumed to be thin so that the thin disk approximation can be applied (e.g. (Popham et al., 1999)), and the analytic solution for the temperature profiles of the disk is utilized (Xue et al., 2013; Liu, Xue, et al., 2016). The neutrino emission occurs at the ignition region of the disk where  $1.473 r_g \leq r \leq 500 r_g$ . We ignore nucleosynthesis when treating the disk consisting of dissociated matter. Under these conditions, the calculations for all disk profiles require significantly less time.

While electron degeneracy is a crucial factor for the thermal distribution (Kohri and Mineshige, 2002; Kohri et al., 2005), maintaining  $Y_e$  in charge-neutrality constraints can be considered instead when  $Y_e$  relates to the perfect equilibrium of neutrons and protons. Under this condition, thermal distribution will primarily rely on temperature, simplifying the luminosity calculation. Our luminosity profiles of the disk are well consistent with previous works, with the maximum luminosity approximately  $10^{53}$  erg  $s^{-1}$  for an extreme accretion rate of  $\dot{m} = 10$  (Popham et al., 1999; Xue et al., 2013; Liu et al., 2017). The peak luminosity is observed at a characteristic radius of  $r \sim 10 r_g$ , where the anti-neutrino emission dominates further in and the neutrino emission dominates further out, comparable to what is presented in (W.-X. Chen and Beloborodov, 2007).

Then, we investigate the annihilation luminosity with and without taking into account neutrino oscillation above the disk. When increasing either  $a$  or  $\dot{m}$ , the neutrino emission (cooling rate) increases. This leads to an increase in the total neutrino luminosity and annihilation luminosity. The annihilation luminosity without oscillation ranges between  $10^{50} - 10^{55}$  erg  $s^{-1}$ , depending on  $a$  and  $\dot{m}$ . Although, in this work, we fix  $r_{\text{in}} = r_{\text{trp}} = 1.473 r_g$  which is the intermediate value reported in (Xue et al., 2013). We also explore the case when  $r_{\text{in}} = 3 r_g$  (Kohri et al., 2005; N. Kawanaka and Mineshige, 2007). The total annihilation luminosity is found to decrease by a factor of  $\sim 2 - 3$  compared to the result obtained when we fix  $r_{\text{in}} = 1.473 r_g$ . Therefore, the choices of  $r_{\text{in}}$  mentioned above do not significantly affect the order of magnitude of the obtained luminosity.

Referring to the pioneering work of (Popham et al., 1999), (Fryer et al., 1999) utilized that result of annihilation luminosity and fitted it in the range of  $\dot{m} = 0.01-0.1$ . Then, (Xue et al., 2013) performed a calculation with a more detailed understanding of neutrino physics. The results of this model are fitted to a wide range of accretion rates  $\dot{m} = 0.01-10$ , while the growth of the luminosity tends to decrease compared to (Fryer et al., 1999). Later, (Liu et al., 2017) extended the numerical solution of (Xue et al., 2013) by including the mass dependence and fitting it in the range of  $\dot{m} = 0.01 - 0.5$ . The fitting line slope of annihilation luminosity is consistent with (Fryer et al., 1999), but the luminosity increases more rapidly than (Xue et al., 2013). The conclusion is that the increase in annihilation luminosity diminishes in high  $\dot{m}$  due to neutrino trapping. In this work, we apply the calculation in (Xue et al., 2013) and fit the annihilation luminosity with  $\dot{m} = 0.1-10$  using linear regression. Our luminosity increases with  $\dot{m}$  analogous to (Xue et al., 2013), but we obtain a greater magnitude of  $\sim 2$  orders. This is due to our oversimplification of electron degeneracy and neutrino trapping effects.

When taking into account the neutrino oscillation in a vacuum above the disk, the flavor transition raises the magnitude of the annihilation luminosity by 12–20% as  $a$  and  $\dot{m}$  decrease. This is because the decrease in energy leads to a higher oscillation frequency and, hence, more frequent flavor transitions. Specifically, transitions from

muon flavor into other flavors occur with high probability. This results in the decrease of the muon neutrino annihilation luminosity by up to 8%, and the increase of the electron- and tau-neutrino luminosities by up to 34% as shown in Table 4.1. Additionally, in higher energy regimes (high  $a$  and  $\dot{m}$ ), the transition from muon flavor is dominated by electron flavor, while in lower energy regimes (low  $a$  and  $\dot{m}$ ) it is dominated by tau flavor. This highlights the important role of energy, which depends on the specific setup of each NDAF model, in dictating neutrino oscillation behavior in this system.

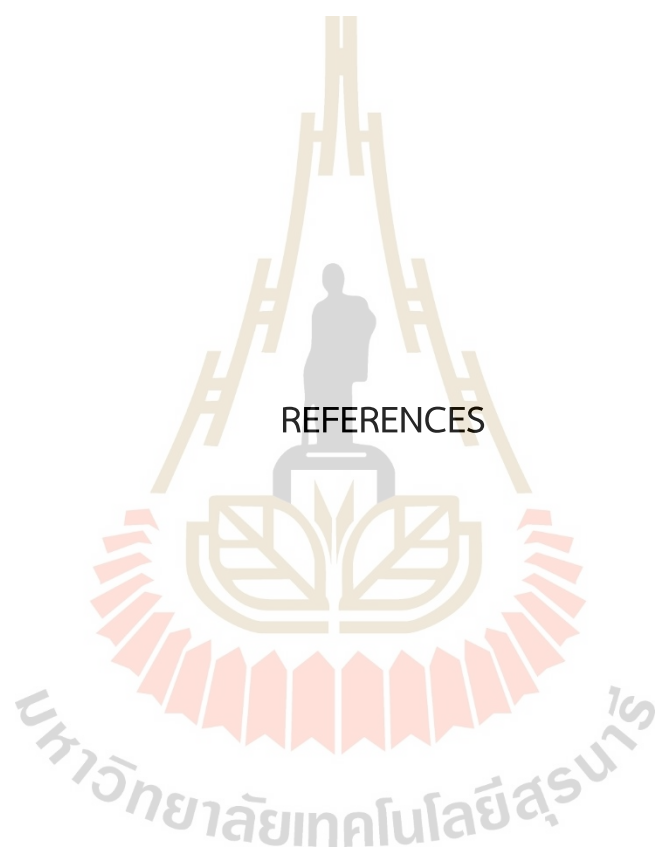
On the other hand, (Uribe et al., 2021) found that the effect of oscillation inside the disk results in the flavor equipartition suppressing the electron neutrino cooling rate but increasing the muon- and tau-neutrino cooling rates. While the model presented in (Uribe et al., 2021) predicts a higher annihilation luminosity compared to other previous works such as (Popham et al., 1999; Xue et al., 2013; Liu et al., 2017), they suggested a decrease in the total annihilation luminosity by as much as 80% due to the neutrino oscillation inside the disk. Therefore, the effect of neutrino oscillation inside the disk (with decreasing luminosity) may compensate for the effect above the disk (with increasing luminosity) so that the net effect is less pronounced. Based on the observed data, the majority of GRB luminosities exceed  $\sim 10^{51}$  erg s<sup>-1</sup> (Pescalli et al., 2016). Therefore, even if we consider the effect of neutrino oscillation, including both inside and above the disk, the energy transferred from annihilation into the relativistic electron-positron outflow may still be sufficient for GRB formation.

The T2K experiment identified CP-violation through the observation of muon flavor transforming into electron flavor for both neutrinos and anti-neutrinos (T2KCollaboration, 2020). In our investigation, we explore scenarios where most muons transition into other flavors, including the CP-violating phase. However, our results suggest that changes in neutrino (anti-neutrino) energies play a more significant role than the CP-violating phase. This is attributed to the higher sensitivity of the oscillation frequency compared to the phase shift. Also, we found that the relative difference in annihilation luminosity between  $\delta CP = 0^\circ$  and  $\delta CP = 245^\circ$  is of the order of  $10^{-4}$ ; this suggests that the CP-violation in vacuum oscillation has minimal impact on

neutrino annihilation. Consequently, detecting the effect of CP-violation on the formation of GRBs remains challenging.

Finally, we suggest that a more comprehensive model, exploring hydrodynamic flow and considering all possible interactions, should be considered. Improvements to the annihilation model could involve incorporating additional effects such as matter oscillation and neutrino-self interaction (Li and Siegel, 2021; Just et al., 2022) with realistic outflow. Additionally, the ray-tracing method (Liu, Zhang, et al., 2016) could be helpful in precisely tracking neutrinos and anti-neutrinos over distances.

As mentioned in Sections 3.4.3.5, the interpretation of neutrino oscillation should be important for flavor transition in the NDAF model. This is because the interactions between neutrinos and antineutrinos with the disk can be considered in a variety of ways. Also, the CP-asymmetry of these particles leads to a different pattern of probability, and this effect accumulates in each step of the mechanism in the model. For future work, we aim to calculate all the possible flavor oscillations of the model, especially inside and above the disk.



REFERENCES

## REFERENCES

- Abbasi, R., Ackermann, M., Adams, J., Ahlers, M., Ahrens, J., Andeen, K., . . . Collaboration, I. (2009). The IceCube data acquisition system: Signal capture, digitization, and timestamping. *Nuclear Instruments and Methods in Physics Research A*, 601, 294-316. doi:10.1016/j.nima.2009.01.001
- Abramowicz, M. A., Czerny, B., Lasota, J. P., and Szuszkiewicz, E. (1988). Slim Accretion Disks. *The Astrophysical Journal*, 332, 646. doi:10.1086/166683
- Ahmad, Q. R., Allen, R. C., Andersen, T. C., D'Anglin, J., Barton, J. C., Beier, E. W., . . . Yeh, M. (2002). Direct Evidence for Neutrino Flavor Transformation from Neutral-Current Interactions in the Sudbury Neutrino Observatory. *Physical Review Letters*, 89(1), 011301. doi:10.1103/PhysRevLett.89.011301
- Becerra, L., Guzzo, M. M., Rossi-Torres, F., Rueda, J. A., Ruffini, R., and Uribe, J. D. (2018). Neutrino Oscillations within the Induced Gravitational Collapse Paradigm of Long Gamma-Ray Bursts. *The Astrophysical Journal*, 852, 120. doi:10.3847/1538-4357/aaa296
- Bellerive, A. (2004). Review of Solar Neutrino Experiments. *International Journal of Modern Physics A*, 19, 1167-1179. doi:10.1142/s0217751x04019093
- Bellerive, A., Klein, J. R., McDonald, A. B., Noble, A. J., and Poon, A. W. P. (2016). The Sudbury Neutrino Observatory. *Nuclear Physics B*, 908, 30-51. doi:10.1016/j.nuclphysb.2016.04.035
- Blandford, R. D., and Znajek, R. L. (1977). Electromagnetic extraction of energy from Kerr black holes. *Monthly Notices of the Royal Astronomical Society*, 179, 433-456. doi:10.1093/mnras/179.3.433
- Caballero, O. L., Zielinski, T., McLaughlin, G. C., and Surman, R. (2016). Black hole spin influence on accretion disk neutrino detection. *Physical Review D*, 93, 123015. doi:10.1103/PhysRevD.93.123015

- Chen, B.-G., Liu, T., Qi, Y.-Q., Huang, B.-Q., Wei, Y.-F., Yi, T., . . . Xue, L. (2022). Effects of vertical advection on multimessenger signatures of black hole neutrino-dominated accretion flows in compact binary coalescences. arXiv:2211.08899.
- Chen, W.-X., and Beloborodov, A. M. (2007). Neutrino-cooled Accretion Disks around Spinning Black Holes. *The Astrophysical Journal*, *657*, 383-399. doi:10.1086/508923
- Cowan, C. L., Reines, F., Harrison, F. B., Kruse, H. W., and McGuire, A. D. (1956). Detection of the Free Neutrino: a Confirmation. *Science*, *124*(3212), 103-104. doi:10.1126/science.124.3212.103
- Davis, R., Harmer, D. S., and Hoffman, K. C. (1968). Search for Neutrinos from the Sun. *Physical Review Letters*, *20*(21), 1205-1209. doi:10.1103/PhysRevLett.20.1205
- Deesamer, C., Chainakun, P., and Sreethawong, W. (2024). Neutrino Oscillation Effects on the Luminosity of Neutrino-Dominated Accretion Flows Around Black Holes. arXiv:2407.20507. doi:10.48550/arXiv.2407.20507
- Di Matteo, T., Perna, R., and Narayan, R. (2002). Neutrino Trapping and Accretion Models for Gamma-Ray Bursts. *The Astrophysical Journal*, *579*, 706-715. doi:10.1086/342832
- Eichler, D., Livio, M., Piran, T., and Schramm, D. N. (1989). Nucleosynthesis, neutrino bursts and  $\gamma$ -rays from coalescing neutron stars. *Nature*, *340*, 126-128. doi:10.1038/340126a0
- Falcone, A., and Collaboration, D. (2022). Deep underground neutrino experiment: DUNE. *Nuclear Instruments and Methods in Physics Research A*, *1041*, 167217. doi:10.1016/j.nima.2022.167217
- Frensel, M., Wu, M.-R., Volpe, C., and Perego, A. (2017). Neutrino flavor evolution in binary neutron star merger remnants. *Physical Review D*, *95*, 023011. doi:10.1103/PhysRevD.95.023011
- Fryer, C. L., Woosley, S. E., Herant, M., and Davies, M. B. (1999). Merging White Dwarf/Black Hole Binaries and Gamma-Ray Bursts. *The Astrophysical Journal*, *520*, 650-660. doi:10.1086/307467



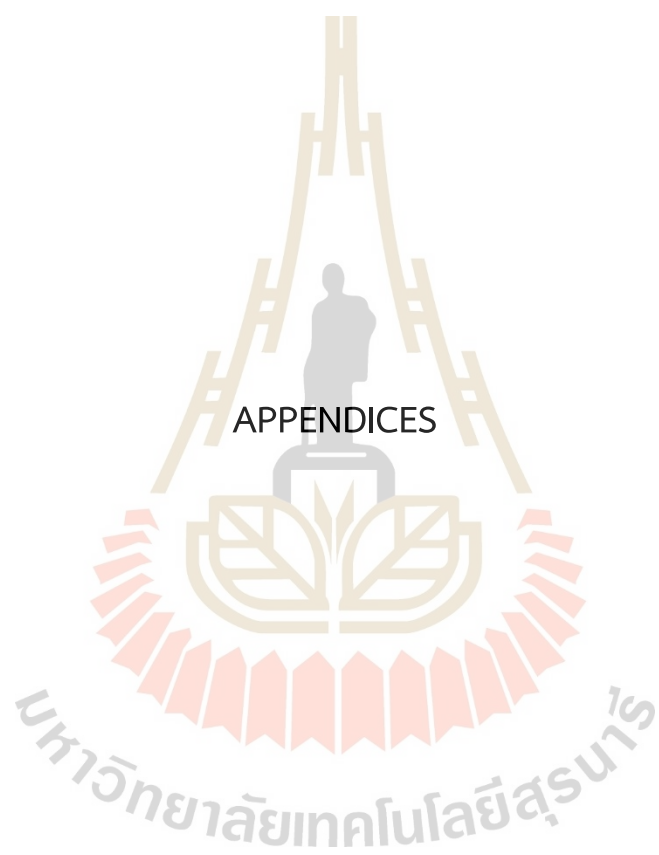
- Fukuda, Y., Hayakawa, T., Ichihara, E., Inoue, K., Ishihara, K., Ishino, H., . . . Young, K. K. (1998). Evidence for Oscillation of Atmospheric Neutrinos. *Physical Review Letters*, *81*(8), 1562-1567. doi:10.1103/PhysRevLett.81.1562
- Gerhardt, L., Klein, S., Stezelberger, T., Barwick, S., Dookayka, K., Hanson, J., and Nichol, R. (2010). A prototype station for ARIANNA: A detector for cosmic neutrinos. *Nuclear Instruments and Methods in Physics Research A*, *624*, 85-91. doi:10.1016/j.nima.2010.09.032
- Gu, W.-M., Liu, T., and Lu, J.-F. (2006). Neutrino-dominated Accretion Models for Gamma-Ray Bursts: Effects of General Relativity and Neutrino Opacity. *The Astrophysical Journal*, *643*, L87-L90. doi:10.1086/505140
- Hawley, J. F., and Krolik, J. H. (2006). Magnetically Driven Jets in the Kerr Metric. *The Astrophysical Journal*, *641*, 103-116. doi:10.1086/500385
- Itoh, N., Hayashi, H., Nishikawa, A., and Kohyama, Y. (1996). Neutrino Energy Loss in Stellar Interiors. VII. Pair, Photo-, Plasma, Bremsstrahlung, and Recombination Neutrino Processes. *The Astrophysical Journal Supplement Series*, *102*, 411. doi:10.1086/192264
- Janiuk, A. (2014). Nucleosynthesis of elements in gamma-ray burst engines. *Astronomy and Astrophysics*, *568*, A105. doi:10.1051/0004-6361/201423822
- Jaroszynski, M. (1996). Hot tori around black holes as sources of gamma ray bursts. *Astronomy and Astrophysics*, *305*, 839. doi:10.48550/arXiv.astro-ph/9506062
- Just, O., Abbar, S., Wu, M.-R., Tamborra, I., Janka, H.-T., and Capozzi, F. (2022). Fast neutrino conversion in hydrodynamic simulations of neutrino-cooled accretion disks. *Physical Review D*, *105*, 083024. doi:10.1103/PhysRevD.105.083024
- Kajita, T. (2010). Atmospheric neutrinos and discovery of neutrino oscillations. *Proceedings of the Japan Academy, Series B*, *86*, 303-321. doi:10.2183/pjab.86.303
- Kawanaka, N., and Masada, Y. (2019). Neutrino-dominated Accretion Flows with Magnetic Prandtl Number-dependent MRI-driven Turbulence. *The Astrophysical Journal*, *881*, 138. doi:10.3847/1538-4357/ab2e71
- Kawanaka, N., and Mineshige, S. (2007). Neutrino-cooled Accretion Disk and Its Stability. *The Astrophysical Journal*, *662*, 1156-1166. doi:10.1086/517985

- Kawanaka, N., Piran, T., and Krolik, J. H. (2013). Jet Luminosity from Neutrino-dominated Accretion Flows in Gamma-Ray Bursts. *The Astrophysical Journal*, 766, 31. doi:10.1088/0004-637x/766/1/31
- Kodama, K., Ushida, N., Andreopoulos, C., Saoulidou, N., Tzanakos, G., Yager, P., . . . Schneps, J. (2001). Observation of tau neutrino interactions. *Physics Letters B*, 504, 218-224. doi:10.1016/s0370-2693(01)00307-0
- Kohri, K., and Mineshige, S. (2002). Can Neutrino-cooled Accretion Disks Be an Origin of Gamma-Ray Bursts? *The Astrophysical Journal*, 577, 311-321. doi:10.1086/342166
- Kohri, K., Narayan, R., and Piran, T. (2005). Neutrino-dominated Accretion and Supernovae. *The Astrophysical Journal*, 629, 341-361. doi:10.1086/431354
- Li, X., and Siegel, D. M. (2021). Neutrino Fast Flavor Conversions in Neutron-Star Postmerger Accretion Disks. *Physical Review Letters*, 126, 251101. doi:10.1103/PhysRevLett.126.251101
- Liu, T., Gu, W.-M., Kawanaka, N., and Li, A. (2015). Vertical Convection in Neutrino-dominated Accretion Flows. *The Astrophysical Journal*, 805, 37. doi:10.1088/0004-637x/805/1/37
- Liu, T., Gu, W.-M., Xue, L., and Lu, J.-F. (2007). Structure and Luminosity of Neutrino-cooled Accretion Disks. *The Astrophysical Journal*, 661, 1025-1033. doi:10.1086/513689
- Liu, T., Gu, W.-M., and Zhang, B. (2017). Neutrino-dominated accretion flows as the central engine of gamma-ray bursts. *New Astronomy Reviews*, 79, 1-25. doi:10.1016/j.newar.2017.07.001
- Liu, T., Xue, L., Zhao, X.-H., Zhang, F.-W., and Zhang, B. (2016). A Method to Constrain Mass and Spin of GRB Black Holes within the NDAF Model. *The Astrophysical Journal*, 821, 132. doi:10.3847/0004-637x/821/2/132
- Liu, T., Zhang, B., Li, Y., Ma, R.-Y., and Xue, L. (2016). Detectable MeV neutrinos from black hole neutrino-dominated accretion flows. *Physical Review D*, 93, 123004. doi:10.1103/PhysRevD.93.123004

- Malkus, A., Kneller, J. P., McLaughlin, G. C., and Surman, R. (2012). Neutrino oscillations above black hole accretion disks: Disks with electron-flavor emission. *Physical Review D*, *86*, 085015. doi:10.1103/PhysRevD.86.085015
- McKinney, J. C., and Gammie, C. F. (2004). A Measurement of the Electromagnetic Luminosity of a Kerr Black Hole. *The Astrophysical Journal*, *611*, 977-995. doi:10.1086/422244
- Meyer, B. S. (1994). The r-, s-, and p-Processes in Nucleosynthesis. *Annual Review of Astronomy and Astrophysics*, *32*, 153-190. doi:10.1146/annurev.aa.32.090194.001101
- Nagataki, S. (2018). Theories of central engine for long gamma-ray bursts. *Reports on Progress in Physics*, *81*, 026901. doi:10.1088/1361-6633/aa97a8
- Narayan, R., Paczynski, B., and Piran, T. (1992). Gamma-Ray Bursts as the Death Throes of Massive Binary Stars. *The Astrophysical Journal*, *395*, L83. doi:10.1086/186493
- Narayan, R., Piran, T., and Kumar, P. (2001). Accretion Models of Gamma-Ray Bursts. *The Astrophysical Journal*, *557*(2), 949. doi:10.1086/322267
- Narayan, R., and Yi, I. (1994). Advection-dominated Accretion: A Self-similar Solution. *The Astrophysical Journal*, *428*, L13. doi:10.1086/187381
- Nunokawa, H., Parke, S., and Valle, J. W. F. (2008). CP violation and neutrino oscillations. *Progress in Particle and Nuclear Physics*, *60*, 338-402. doi:10.1016/j.pnnp.2007.10.001
- Paczynski, B. (1991). Cosmological gamma-ray bursts. *Acta Astronomica*, *41*, 257-267.
- Paczynski, B., and Xu, G. (1994). Neutrino Bursts from Gamma-Ray Bursts. *The Astrophysical Journal*, *427*, 708. doi:10.1086/174178
- Pan, Z., and Yuan, Y.-F. (2012). Vertical Structure of Neutrino-dominated Accretion Disks and Neutrino Transport in the Disks. *The Astrophysical Journal*, *759*, 82. doi:10.1088/0004-637x/759/2/82
- Pescalli, A., Ghirlanda, G., Salvaterra, R., Ghisellini, G., Vergani, S. D., Nappo, F., . . . Götz, D. (2016). The rate and luminosity function of long gamma ray bursts. *Astronomy and Astrophysics*, *587*, A40. doi:10.1051/0004-6361/201526760

- Pontecorvo, B. (1958). Mesonium and Antimesonium. *Soviet Journal of Experimental and Theoretical Physics*, 6, 429. Retrieved from <https://ui.adsabs.harvard.edu/abs/1958JETP....6..429P>
- Popham, R., Woosley, S. E., and Fryer, C. (1999). Hyperaccreting Black Holes and Gamma-Ray Bursts. *The Astrophysical Journal*, 518(1), 356. doi:10.1086/307259
- Rosswog, S., Ramirez-Ruiz, E., and Davies, M. B. (2003). High-resolution calculations of merging neutron stars - III. Gamma-ray bursts. *Monthly Notices of the Royal Astronomical Society*, 345, 1077-1090. doi:10.1046/j.1365-2966.2003.07032.x
- Ruffert, M., and Janka, H.-T. (1999). Gamma-ray bursts from accreting black holes in neutron star mergers. *Astronomy and Astrophysics*, 344, 573-606. doi:10.48550/arXiv.astro-ph/9809280
- Seitenzahl, I. R., Timmes, F. X., Marin-Lafleche, A., Brown, E., Magkotsios, G., and Truran, J. (2008). Proton-rich Nuclear Statistical Equilibrium. *The Astrophysical Journal*, 685, L129. doi:10.1086/592501
- Shakura, N. I., and Sunyaev, R. A. (1973). Black holes in binary systems. Observational appearance. *Astronomy and Astrophysics*, 24, 337-355.
- She, J.-Z., Liu, T., and Xue, L. (2022). Relativistic global solutions of neutrino-dominated accretion flows with magnetic coupling. *Monthly Notices of the Royal Astronomical Society*, 513, 3960-3970. doi:10.1093/mnras/stac1154
- T2K Collaboration. (2020). Constraint on the matter-antimatter symmetry-violating phase in neutrino oscillations. *Nature*, 580, 339-344. doi:10.1038/s41586-020-2177-0
- Tian, J. Y., Patwardhan, A. V., and Fuller, G. M. (2017). Neutrino flavor evolution in neutron star mergers. *Physical Review D*, 96, 043001. doi:10.1103/PhysRevD.96.043001
- Uribe, J. D., Becerra-Vergara, E. A., and Rueda, J. A. (2021). Neutrino Oscillations in Neutrino-Dominated Accretion Around Rotating Black Holes. *Universe*, 7, 7. doi:10.3390/universe7010007
- Wei, Y.-F., and Liu, T. (2022). Black Hole Hyperaccretion in Collapsars. III. GRB Timescale. *The Astrophysical Journal*, 936, 182. doi:10.3847/1538-4357/ac8bd1

- Woosley, S. E., and Bloom, J. S. (2006). The Supernova Gamma-Ray Burst Connection. *Annual Review of Astronomy and Astrophysics*, 44, 507-556. doi:10.1146/annurev.astro.43.072103.150558
- Workman, R. L., Burkert, V. D., Crede, V., Klempt, E., Thoma, U., Tiator, L., . . . Group, P. D. (2022). Review of Particle Physics. *Progress of Theoretical and Experimental Physics*, 2022, 083C001. doi:10.1093/ptep/ptac097
- Wu, M.-R., and Tamborra, I. (2017). Fast neutrino conversions: Ubiquitous in compact binary merger remnants. *Physical Review D*, 95, 103007. doi:10.1103/PhysRevD.95.103007
- Xue, L., Liu, T., Gu, W.-M., and Lu, J.-F. (2013). Relativistic Global Solutions of Neutrino-dominated Accretion Flows. *The Astrophysical Journal Supplement Series*, 207, 23. doi:10.1088/0067-0049/207/2/23
- Yokoyama, M. (2017). The Hyper-Kamiokande Experiment. arXiv:1705.00306. doi:10.48550/arXiv.1705.00306
- Zalamea, I., and Beloborodov, A. M. (2011). Neutrino heating near hyper-accreting black holes. *Monthly Notices of the Royal Astronomical Society*, 410, 2302-2308. doi:10.1111/j.1365-2966.2010.17600.x



## APPENDIX A

### NEUTRINO EMISSION

This following section is from the manuscript, titled “Neutrino Oscillation Effects on the Luminosity of Neutrino-Dominated Accretion Flows Around Black Holes”. It was originally included there in Appendix A, the “NEUTRINO EMISSION” and “OSCILLATION PARAMETERS”. The manuscript is now under revision for publication in The Astrophysical Journal (ApJ) in 2024, article in press.

The major cross sections from scattering off electrons, free protons, free neutrons and other elements particles are given by (Liu et al., 2017),

$$\sigma_{e,\nu_i} = \frac{3k_B T \sigma_0 E_{\nu_i}}{8m_e c^2} \left(1 + \frac{\eta_e}{4}\right) \left[ (C_{V,\nu_i} + C_{A,\nu_i})^2 + \frac{1}{3} (C_{V,\nu_i} - C_{A,\nu_i})^2 \right], \quad [20]$$

$$\sigma_{n_1,\nu_i} = \frac{\sigma_0 E_{\nu_i}^2}{4} \left[ (C_{V,\nu_i} - 1)^2 + 3g_A^2 (C_{A,\nu_i} - 1)^2 \right], \quad [21]$$

$$\sigma_{n_2,\nu_i} = \frac{\sigma_0 E_{\nu_i}^2}{4} \frac{1+3g_A^2}{4}, \quad [22]$$

$$\sigma_{n_j,\nu_i} = \frac{\sigma_0 E_{\nu_i}^2}{16} (Z_j + N_j) \left[ 1 - \frac{2Z_j}{Z_j + N_j} (1 - 2 \sin^2 \theta_W) \right]^2, \quad [23]$$

where  $\sigma_0 = 4G_F^2 (m_e c^2)^2 / \pi (\hbar c)^4 \approx 1.71 \times 10^{-44} \text{ cm}^2$ ,  $G_F \approx 1.436 \times 10^{-49} \text{ erg cm}^3$ ,  $E_{\nu_i}$  is the mean energy of neutrinos in unit of  $(m_e c^2)$ ,  $g_A \approx 1.26$ ,  $\sin^2 \theta_W \approx 0.23$ ,  $Z_j$  and  $N_j$  are defined as the number of proton and neutrons of a nucleus  $X_j$ , and  $C_{V,\nu_e} = 1/2 + 2 \sin^2 \theta_W$ ,  $C_{V,\nu_\mu} = C_{V,\nu_\tau} = -1/2 + 2 \sin^2 \theta_W$ ,  $C_{A,\nu_e} = C_{A,\bar{\nu}_\mu} = C_{A,\bar{\nu}_\tau} = 1/2$ , and  $C_{A,\bar{\nu}_e} = C_{A,\nu_\mu} = C_{A,\nu_\tau} = -1/2$ .

$$q_{\nu_i} = q_{Urca} + q_{e^- + e^+ \rightarrow \nu_i + \bar{\nu}_i} + q_{n + n \rightarrow n + n + \nu_i + \bar{\nu}_i} + q_{\bar{\nu}_i \rightarrow \nu_i + \bar{\nu}_i}. \quad [24]$$

First,  $q_{Urca}$  is from the Urca process included in the proton-rich NSE (Xue et al., 2013). This process plays an important role in neutrino radiation and relates only to electron neutrino. There are four major terms for electrons, positrons, free protons, free neutrons and nucleons (N. Kawanaka and Mineshige, 2007; Liu et al., 2007), which are expressed by

$$q_{Urca} = q_{p+e^- \rightarrow n+\nu_e} + q_{n+e^+ \rightarrow p+\bar{\nu}_e} + q_{n \rightarrow p+e^- + \bar{\nu}_e} + q_{X_j + e^- \rightarrow X'_j + \nu_e}, \quad [25]$$

with



$$q_{p+e^- \rightarrow n+\nu_e} = \frac{G_F^2 \cos^2 \theta_c}{2\pi^2 \hbar^3 c^2} (1 + 3g_A^2) n_1 \times \int_Q^\infty \sqrt{E_e^2 - m_e^2 c^4} (E_e - Q)^3 f(E_e, \eta_e) E_e dE_e, \quad [26]$$

$$q_{n+e^+ \rightarrow p+\bar{\nu}_e} = \frac{G_F^2 \cos^2 \theta_c}{2\pi^2 \hbar^3 c^2} (1 + 3g_A^2) n_2 \times \int_{m_e c^2}^\infty \sqrt{E_e^2 - m_e^2 c^4} (E_e + Q)^3 f(E_e, -\eta_e) E_e dE_e, \quad [27]$$

$$q_{n \rightarrow p+e^-+\bar{\nu}_e} = \frac{G_F^2 \cos^2 \theta_c}{2\pi^2 \hbar^3 c^2} (1 + 3g_A^2) n_2 \times \int_{m_e c^2}^Q \sqrt{E_e^2 - m_e^2 c^4} (Q - E_e)^3 [1 - f(E_e, \eta_e)] E_e dE_e, \quad [28]$$

$$q_{X_j+e^- \rightarrow X'_j+\nu_e} = \frac{G_F^2 \cos^2 \theta_c}{2\pi^2 \hbar^3 c^2} g_A^2 \frac{2}{7} N_p(Z_j) N_h(N_j) n_j \times \int_{Q'}^\infty \sqrt{E_e^2 - m_e^2 c^4} (E_e - Q')^3 f(E_e, \eta_e) E_e dE_e, \quad [29]$$

where  $\cos^2 \theta_c \approx 0.947$ ,  $Q = (m_n - m_p)c^2$ ,  $Q' \approx \mu'_n - \mu'_p + \Delta$ ,  $\mu'_n$  and  $\mu'_p$  are the chemical potential of protons and neutrons in their own nuclei,  $\Delta \approx 3$  MeV is the energy of the neutron  $1f_{5/2}$  state above the ground state.  $f(E, \eta)$  is the Fermi-Dirac distribution function given by

$$f(E, \eta) = \frac{1}{e^{(E/k_B T) - \eta} + 1}, \quad [30]$$

where  $E$  is the energy in unit  $(m_e c^2)$ ,

$$N_p(Z_j) = \begin{cases} 0, & Z_j < 20 \\ Z_j - 20, & 20 < Z_j < 28, \\ 8, & Z_j > 28, \end{cases} \quad [31]$$

$$N_h(N_j) = \begin{cases} 6, & N_j < 34, \\ 40 - N_j, & 34 < N_j < 40, \\ 0, & N_j > 40. \end{cases} \quad [32]$$

The second process is from the electron-positron pair annihilation into neutrinos  $q_{e^-+e^+ \rightarrow \nu_i+\bar{\nu}_i}$ . This term can be neglected when electrons are in a degenerate state (Kohri et al., 2005).

The third one is from the nucleon-nucleon bremsstrahlung  $q_{n+n \rightarrow n+n+\nu_i+\bar{\nu}_i}$ . The rate is the same for three flavors of neutrinos (Itoh, Hayashi, Nishikawa, and Kohyama, 1996; Di Matteo et al., 2002; Liu et al., 2017),

$$q_{n+n \rightarrow n+n+\nu_i+\bar{\nu}_i} \approx 1.5 \times 10^{27} \rho_{10}^2 T_{11}^{5.5} \text{ erg cm}^{-3} \text{ s}^{-1}. \quad [33]$$

The final main process is the plasmon decay  $q_{\tilde{\gamma} \rightarrow \nu_i+\bar{\nu}_i}$ , where plasmons  $\tilde{\gamma}$  are photons interacting with electrons (N. Kawanaka and Mineshige, 2007),

$$q_{\tilde{\gamma} \rightarrow \nu_e+\bar{\nu}_e} = \frac{\pi^4}{6\alpha^*} C_{V,\nu_e} \frac{\sigma_0 c}{(m_e c^2)^2} \frac{(k_B T)^9}{(2\pi \hbar c)^6} \gamma^6 \times (\gamma^2 + 2\gamma + 2) \exp(-\gamma), \quad [34]$$

$$q_{\tilde{\gamma} \rightarrow \nu_\mu + \bar{\nu}_\mu} = q_{\tilde{\gamma} \rightarrow \nu_\tau + \bar{\nu}_\tau} = \frac{4\pi^4}{6\alpha^*} C_{V,\nu_\mu} \frac{\sigma_0 c}{(m_e c^2)^2} \frac{(k_B T)^9}{(2\pi\hbar c)^6} \gamma^6 \times (\gamma^2 + 2\gamma + 2) \exp(-\gamma), \quad [35]$$

$\alpha^* \approx 1/137$  is the fine-structure constant and  $\gamma \approx 5.565 \times 10^{-2} [(\pi^2 + 3\eta_e^2)/3]^{1/2}$ .



## APPENDIX B

### OSCILLATION PARAMETERS

This following section is from the manuscript, titled “Neutrino Oscillation Effects on the Luminosity of Neutrino-Dominated Accretion Flows Around Black Holes”. It was originally included there in appendix A, the “NEUTRINO EMISSION” and “OSCILLATION PARAMETERS”. The manuscript is now under revision for publication in The Astrophysical Journal (ApJ) in 2024, article in press.

Without considering the matter oscillation, self-interaction, and/or other interactions, the neutrino oscillation is calculated in the vacuum limit. If one assumes that the neutrino is not Majorana particle, the unitary transformation for any flavors is described by the Pontecorvo–Maki–Nakagawa–Sakata matrix (PMNS matrix) given by

$$U = \begin{pmatrix} c_{12}c_{23} & s_{12}c_{23} & s_{13}e^{-i\delta_{CP}} \\ -s_{12}c_{23} - c_{12}s_{23}s_{13}e^{i\delta_{CP}} & c_{12}c_{23} - s_{12}s_{13}s_{23}e^{i\delta_{CP}} & c_{13}s_{23} \\ s_{12}s_{23} - c_{12}c_{23}s_{13}e^{i\delta_{CP}} & -c_{12}s_{23} - s_{12}s_{13}c_{23}e^{i\delta_{CP}} & c_{13}c_{23} \end{pmatrix}, \quad [36]$$

where  $c_{\alpha\beta} = \cos \theta_{\alpha\beta}$ , and  $s_{\alpha\beta} = \sin \theta_{\alpha\beta}$ , and the values  $\theta_{12} = 33.65^\circ$ ,  $\theta_{23} = 47.64^\circ$ , and  $\theta_{13} = 8.53^\circ$ , are taken from PDG.

## CURRICULUM VITAE

**Name** : Chitipat Deesamer

**Date of Birth** : 29/11/1998

**Place of Birth** : Surin, Thailand

**Residence** : 292/12 Pattamanon Road, Nai-Mueang Sub-district, Mueang Surin District, Surin 32000, Thailand

**Tel** : +66-833697513

### Education

2017-2020 : Bachelor of Science, School of Physics, Institute of Science, Suranaree University of Technology

2020-present : Master of Science, School of Physics, Institute of Science, Suranaree University of Technology

### Publication

1. Luangtip, W., Chainakun, P., Loekkesee, S., Deesamer, C., Ngonsamrong, T., and Sintusiri, T. (2021). X-ray reverberation models of the disc wind in ultraluminous X-ray source NGC 5408 X-1. *Monthly Notices of the Royal Astronomical Society*, 507, 6094-6107. doi:10.1093/mnras/stab2494
2. Deesamer, C., Chainakun, P., and Sreethawong, W. (2024). Neutrino Oscillation Effects on the Luminosity of Neutrino-dominated Accretion Flows around Black Holes. *The Astrophysical Journal*, 973(2), 165. doi:10.3847/1538-4357/ad68f5